FACULTY OF SCIENCE AND TECHNOLOGY

MASTER'S THESIS

Study programme / specialisation: Engineering Structures and Materials- Master's Degree Programme/ Structural Engineering	Spring, 2023 Open / Confidential: Open
Author: Torstein Ulland Dirdal	
Supervisor at UiS: Yanyan Sha	
Thesis title: Dropped object impact analysis on subsea pipelines	
Credits (ECTS): 30	
Keywords: LS-DYNA Dropped Object Subsea Pipeline	Pages: 64 Stavanger, *15.06.2023*

Preface

This master's thesis was written to finish my master's in Structural and Mechanical Engineering at the University of Stavanger (UiS). This thesis aimed to gain more knowledge on the topic surrounding dropped objects. Associate Professor Yanyan Sha proposed the subject.

I applied to write about this subject since I found it very interesting, and it was a topic I didn't know much about in advance. I was also eager to learn a new modelling software like LS-DYNA.

I want to thank my supervisor, Yanyan Sha, for helping me through this period and helping me with guidance and motivation in the subject. I am also grateful for all the help I received to understand and gain as much knowledge as possible about LS-DYNA.

I want to thank DYNAmore and Axel Hallén for setting up and holding a good beginner's course in LS-DYNA. This provided me with the necessary knowledge to design my models.

The simulations were performed on resources provided by Sigma2 - the National Infrastructure for High Performance Computing and Data Storage in Norway.

I would also like to thank Aker Solutions for letting me use their designed container model in the analysis.

Abstract

This thesis studies the response of a subsea pipeline's structure when a dropped object hits it. The pipeline and seabed were modelled using solid elements, while the container model was imported from Aker Solutions and is composed of shell elements. LS-DYNA, a finite element software, was used to conduct the analysis. The key parameters studied in this research were impact force, internal energy, and pipeline deformation. Thirteen different cases have been analysed in addition to three cases used in a mesh convergence test. The impact scenarios have been described in Table 8, Chapter 4.11 and the three mesh convergence cases have been described in Table 9, Chapter 4.11.

The thesis includes a literature study of relevant standards and previous research that has been conducted. DNVGL-RP-C204 and DNVGL-RP-F107 are the applicable standards for dropped objects in this thesis. DNVGL-RP-C204 provides essential information on calculating impact velocity, dissipation of strain energy, and force-deformation curve for tubular members. At the same time, DNVGL-RP-F107 presents information on drop probability in crane lifting operations, the hit probability onto a subsea pipeline, and various protection methods available in the industry.

A mesh convergence study was carried out to determine the optimal mesh size for the models. This involved comparing three models with the same properties, apart from the mesh size, and observing at which mesh size the outcome converged. The objective was to identify the largest feasible mesh size that would have little to no impact on the precision of the results.

A comprehensive parametric study of the subsea pipeline was conducted to analyse its response to the different cases. This involved testing for various scenarios on the pipeline under different conditions, such as altering the soil parameters, protection method, yield strength, and the impact angle of the container. The container's velocity was kept constant at 10 m/s in all the impact scenarios. The impact angle was identified as a crucial factor in the extent of damage inflicted on the pipeline. The use of concrete coating reduced the deformation and the internal energy in the pipeline. With a flexible seabed, the internal energy was reduced for the scenario with coating. However, that was not the case for the unprotected pipeline. The possible reason is explained in this thesis. By increasing the pipeline’s yield strength, the internal energy and deformation of the pipeline were significantly reduced.

Sammendrag

I denne masteroppgaven fokuseres det på å studere responsen til en undersjøisk rørledning når den blir truffet av et fallende objekt. Modelleringen av rørledningen og havbunnen ble gjort ved hjelp av solide elementer, mens container modellen ble importert fra Aker Solutions og består av flere skall-elementer. LS-DYNA, en programvare for elementanalyser, er blitt brukt til å utføre analysen. De viktigste parameterne som studeres i denne oppgaven, er slagkraft, intern energi og deformasjon av røret. Tretten ulike tilfeller er blitt analysert i tillegg til tre scenarier brukt i en mesh-konvergens test. De tretten tilfellene er beskrevet i Tabell 8, kapittel 4.11, og de tre mesh-konvergens tilfellene er beskrevet i Tabell 9, kapittel 4.11.

Videre tar oppgaven for seg en litteraturstudie av relevante standarder og tidligere forskning. DNVGL-RP-C204 og DNVGL-RP-F107 er de aktuelle standardene for fallende objekter i denne oppgaven. DNVGL-RP-C204 gir essensiell informasjon om beregning av hastighet ved kollisjon, fordelingen av spenningsenergi og kraft-deformasjonskurve for rørformede komponenter. Samtidig presenterer DNVGL-RP-F107 informasjon om sannsynligheten for fall ved kranløfteoperasjoner, treffsannsynligheten til et fallende objekt og ulike beskyttelsesmetoder som er tilgjengelige i industrien.

For å bestemme best mulig meshstørrelse for modellene, ble det utført en konvergenstest. Dette innebar å sammenligne resultatene til tre modeller hvor den eneste forskjellen var meshstørrelsen. Nødvendig meshstørrelse ble bestemt utifra når resultatene startet å konvergere. Målet var å identifisere den største mulige meshstørrelsen som ville ha liten eller ingen innvirkning på presisjonen av resultatene.

Videre ble det gjennomført en omfattende parametrisk studie av den undersjøiske rørledningen for å analysere responsen i ulike scenarier. Dette innebar testing av ulike scenarier for rørledningen under forskjellige forhold, for eksempel endring av sjøbunnsparametere, beskyttelsesmetode, stålets flytegrense og kollisjonsvinkelen til containeren. Gjennom alle scenarier ble containerens hastighet holdt konstant på 10 m/s. Kollisjonsvinkelen ble identifisert som en avgjørende faktor med tanke på omfanget av skade påført rørledningen. Ved bruk av betongbeskyttelse ble deformasjonen og den interne energien i røret redusert. Med en fleksibel sjøbunn ble den interne energien redusert for scenariet med betongbeskyttelse. Dette var imidlertid ikke tilfelle for den ubeskyttede rørledningen. Den mulige årsaken er forklart i denne

oppgaven. Ved en økning av rørets flytegrense ble den interne energien og deformasjonen betydelig redusert.

Table of Contents

List of Figures

List of Tables

1 Introduction

The risk of dropped objects is highly relevant in the offshore business due to the increasing number of offshore operations in the past few decades. With more offshore activity, the risk of an accident increases [1].

Oil and gas platform operations constitute a significant contributor regarding dropped object accidents. There are also some extra concerns regarding the consequence of an object falling into the sea near these platforms. The consequences can be serious if a dropped object hits one of the surrounding subsea pipelines transporting oil and gas. These accidents may result in casualties, significant economic losses, and/or pollution from oil and gas. This can, in turn, affect the marine life in the area [1]. In this thesis, only accidents where objects fall into the sea are considered.

Figure 1 - Damage done to a pipeline by a dropped object [2]

The thesis will give an overview of the probability of a dropped object accident occurring, and the chances of the object hitting a subsea pipeline, based on DNV-RP-F107 [3]. Since an object falling into the sea will not have a straight trajectory, an overview of the expected course based on the DNV-RP-F107 standard has been given. A summary of pipeline protection has also been described based on the same standard.

The standard DNV-RP-C204 presents an overview of impact velocity, dissipation of strained energy and the force-deformation relationship between the dropped object and the impacted member [4].

This thesis focuses on a model container designed by Aker Solutions. The model container hits a model pipeline lying partly buried on the seabed. The pipeline was designed as a steel central part with a concrete protection around the pipe. The container has been modelled as several shell elements. LS-DYNA has been used in the modelling. The thesis will investigate how different types of angles, protection, seabed, and yield strength will affect the internal energy, impact force and the deformation of the pipeline. LS-DYNA has been applied for numerical analyses and for comparison of the various scenarios examined.

1.2 Problem Thesis

The thesis aims to investigate how a subsea pipeline reacts to different impact scenarios, and compare results in order to gain more knowledge regarding dropped object accidents.

1.3 Challenges

One of the main challenges was the need to learn a new software for designing the models. Modelling and getting all the scenarios working took more time than expected. Also, the amount of storage required, and the computational time were a problem initially, creating even more delays. When the models worked correctly, a supercomputer was utilised to run the analyses. This reduced the run time significantly, as compared to using LS-Run.

Another challenge was to choose the correct material property for the different parts. This was important for the model to act as intended and took some time to manage properly.

1.4 Limitations

The master's thesis is limited to considering a subsea pipeline's structural response when subjected to a container impact. Other possible impacts, such as pipes or tanks are not considered. The thesis only evaluates and compares one protection method vs an unprotected pipeline.

Additionally, the container is assumed to be moving at a constant velocity, and the possible effects of object excursion and hydrodynamics are not considered in this study.

The number of scenarios evaluated has been limited to a total of sixteen, and the mesh sizes considered are constrained by the available computational power. Finally, the material used for the container has been kept constant, as designed by Aker Solutions.

2 Literature Review and Design Codes

2.1 Previous Research

Research has been done on different problems surrounding dropped objects in the offshore business.

A research paper by Z. Liu and A.K. Verma [5] has investigated the probability of a dropped object hitting a subsea pipeline. The DNVGL-RP-F107 standard uses the “ring model” to quantify this kind of risk. The “ring model” uses a breadth interval of 10 meters. This paper investigates the sensitivity of the breadth interval and how it affects the hit probability. The hit probability was found to start converging when the breadth interval is lower than 5 meters. The normalised 10-meter breadth interval used in the standard tends to give a higher total hit probability [5].

The trajectory of a falling object is investigated in an article by G. Xiang et al. [1] . The article provides an overview and analysis of the recent research and challenges of dropped objects in offshore engineering. In general, the falling trajectory can be divided into three phases: the air-falling stage, the water-entry stage and the underwater sinking stage. In the air-falling stage, the object is mainly subjected to external forces, such as gravitational force and air resistance. The water entry stage involves more advanced mechanisms like jet flow and splashing. This stage is further divided into four phases: the shake phase, the flow forming phase, the open cavity phase, and the closed cavity phase. The underwater sinking stage is mostly affected by upward and downward forces. The object has reached terminal velocity when these two forces are equal [1]. The article focuses on the underwater sinking stage.

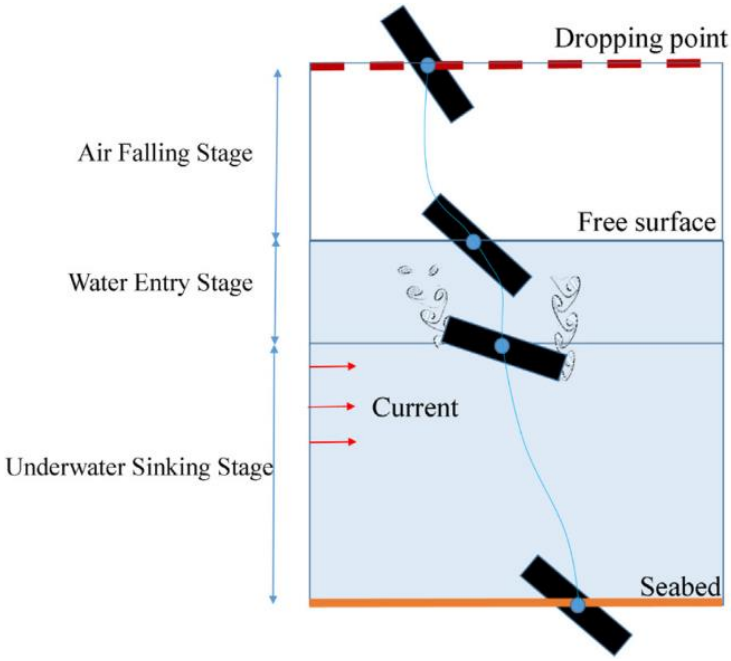

Figure 2 - Stages of a falling object in water [1]

A. Ramberg has written a master's thesis regarding dropped objects on offshore installations [6]. The thesis investigates the structural response of a stiffened panel due to impact from a dropped object, focusing on a falling container. The study focuses on how different impact scenarios affect the stiffened panel and container. A modelling software called Abaqus was utilised to model both a container and stiffened panel.

An article investigating the deformation response of submarine pipelines subjected to impact loads by dropped objects has been written by F. Jiang et al. [7]. The article examines how the effects of impact velocity, dropped object mass and shape, pipeline thickness and coating, and the seabed flexibility affect the deformation of the pipeline. It also considers the optimal burial depth, concluding that the pipeline is most vulnerable when it is semi-buried in the seabed.

An article written by M. R. U Kawsar et al. [8] studies the effect of different objects and impact angles on a corroded subsea pipeline, focusing on risk assessment. The study uses a probabilistic and numerical model to analyse different accidental scenarios and to evaluate the safety of a pipeline exposed to these.

2.2 DNV Standards

There are, in general, two standards that are relevant to this topic. In this thesis, the following are mentioned:

- DNVGL-RP-C204- Design against accidental loads [4]
- DNVGL-RP-F107- Risk assessment of pipeline protection [3]

2.2.1 Drop Probability

The section regarding drop probability can be found in DNVGL-RP-F107, section 5 [3]. To determine the likelihood of a drop, the UK Department of Energy has gathered data on accidents from 1980-1986. It has been estimated that approximately 3.7 million lifts were performed in this period, which corresponds to 4500 lifts per crane per year. The data shows the dropped object incidents to be 81, where around 70% of the drops fell onto the deck, and 30% fell into the sea.

Table 1 shows the frequency of dropped objects falling into the sea with different lift operations [3].

Table 1 - Frequencies for dropped objects into the sea [3]

Type of lift	**Frequency of dropped objects into the sea (per lift)**
Ordinary lift to/from supply vessel with platform crane < 20 tonnes	$1.2 * 10^{-5}$
Heavy lift to/from supply vessel with the platform crane > 20 tonnes	$1.6 * 10^{-5}$
Handling of load < 100 tonnes with the lifting system in the drilling derrick	$2.2 * 10^{-5}$
Handling of BOP/load > 100 tonnes with the lifting system in the drilling derrick	$1.5 * 10^{-3}$

2.2.2 Object Excursion and Hit Probability

The falling pattern is highly dependent on the shape and weight of the falling object, as well as the angle of impact with the sea surface. Other parameters may also affect the object excursion, as mentioned by G. Xiang et al. [1]. The section regarding object excursion and hit probability is described in DNVGL-RP-F107 [3].

One way of calculating the probability of a sinking object hitting the sea bottom at a distance *x* from the vertical line is by using equation 1 [3]. The calculation depends on the horizontal distance to the sea bottom *x* and the lateral deviation δ.

$$p(x) = \frac{1}{\sqrt{2\pi}\delta} e^{-\frac{1}{2}\left(\frac{x}{\delta}\right)^2} \quad (1)$$

After calculating *p(x)*, the probability of the object hitting the seabed within a certain area can be established. To calculate this probability, equation 2 is used. This calculation depends on the distance *r* from the vertical line through the drop point, and *p(x)* [3].

$$P(x \leq r) = \int_{-r}^{r} p(x)dx \quad (2)$$

The probability of the object hitting within a ring (see Figure 3) can be calculated using a ring model. Each ring typically has a 10-meter breadth interval, as given in DNVGL-RP-F107 [3]. However, according to Z. Liu and A.K. Verma [5], this interval could be advantageously reduced to as low as 5 meters.

Equation 3 may be used for this calculation [3]:

$$P_{hit,r} = P(r_i < x \leq r_o) = P(x \leq r_o) - P(x \leq r_i) \quad (3)$$

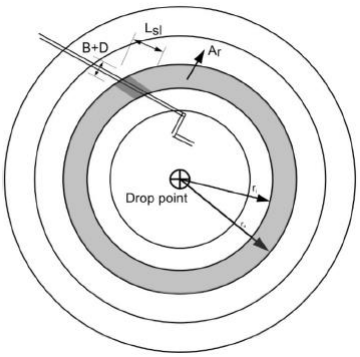

Figure 3 - Ring model [9]

Equation 4 can be used to calculate the probability of an object hitting a subsea pipeline within a particular ring $P_{hit,sl,r}$ [3]. The formula is dependent on the probability of impact within the

ring $P_{hit,r}$, the length of the subsea line within the circle L_{sl}, the diameter of the subsea line *D*, the breadth of a falling object *B* and the area within the specific ring A_r.

$$P_{hit,sl,r} = P_{hit,r} * \frac{L_{sl} * (D + B)}{A_r} \tag{4}$$

2.2.3 Impact Velocity

The section regarding impact velocity is described in DNGL-RP-C204, section 4.2 [4]. The kinetic energy of a given object is governed by the mass of the object *m*, the hydrodynamic added mass m_a and the object's terminal velocity v_t. The kinetic energy of a falling object in water is given by equation 5.

$$E_{kin} = \frac{1}{2} * (m + m_a) * {v_t}^2 \tag{5}$$

The terminal velocity is the maximum velocity an object can obtain while falling through a fluid. This is obtained when the drag and buoyancy forces balance the gravity force [4]. To find the terminal velocity, numerous factors need consideration. Factors such as the density of water p_w, hydrodynamic drag coefficient C_d, the projected cross-sectional area of the object A_p and the object displacement *V* need to be found [4]. The terminal velocity is given by equation 6.

$$v_t = \sqrt{\frac{2g * (m - p_w * V)}{p_w * C_d * A_p}} \tag{6}$$

The travelled distance must be considered to calculate when the object reaches its terminal velocity. Factors such as mass, added mass, the density of water, drag coefficient and the projected cross-sectional area of the object need to be considered. The travelled distance is given by equation 7.

$$s_c = \frac{m + m_a}{p_w * C_d * A_p} \tag{7}$$

2.2.4 Dissipation of Strain Energy

Strain energy is the stored potential energy contained in a material subjected to a load [11]. The dissipation of strain energy is a suitable measurement to determine how much energy the

container and the pipeline absorb. The strain energy dissipation may be found from the relationship between the dropped object and the impacted member as a force-deformation relation. This results from the dissipation of elastic and plastic strain energy [10]. Figure 4 shows a representation of the resistance for the dropped object and the impacted member, where the strain energy of a dropped object $E_{s,o}$, the strain energy of impacted material $E_{s,i}$, the load of dropped object R_o, the load of impacted member R_i, the deformation of a dropped object w_o and the deformation of the impacted member w_i is represented. The area under the two graphs represents the respective dissipated strain energies [4]. The section regarding strain energy dissipation can be found in DNVGL-RP-C204, section 4.3 [4].

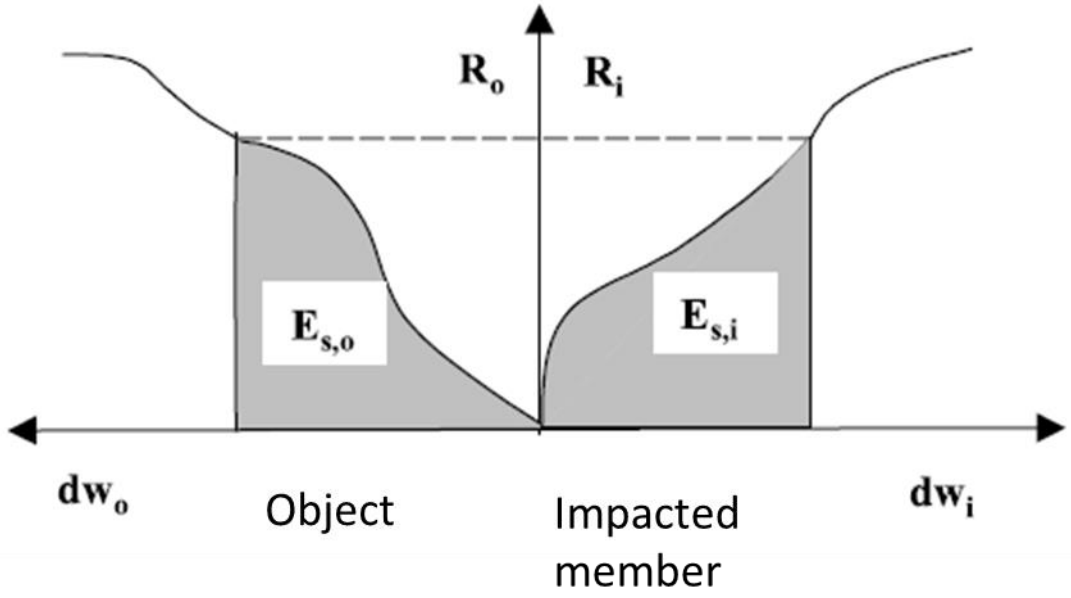

Figure 4 - Force vs deformation for container and pipeline [4]

The total dissipated energy E_s can be found by integrating the two force-deformation curves. This is done to find the area under the curves corresponding to the total dissipated energy [4]. An expression to calculate the total dissipated energy is given by equation 8.

$$E_s = E_{s,o} + E_{s,i} = \int_0^{w_{0,max}} R_o dw_o + \int_0^{w_{i,max}} R_i dw_i \tag{8}$$

2.2.5 Force-deformation Curve for Tubular Members

The section regarding the force-deformation curve for tubular members can be found in DNVGL-RP-C204 , section 3.6 [4]. The local denting resistance of a tubular member can be calculated analytically using several methods. In this chapter, two of these procedures will be proposed. DNV-RP-C204 proposes to use Figure 5 to calculate the resistance to indentation of

unstiffened tubes [4]. The calculation can be done by looking at the relationship between the dent depth w_d and the diameter of the hit cross-section D. The width of the contact area B in relation to the hit cross-section also needs to be considered. After finding the two values, the local denting resistance can be found [4].

Using Figure 5 to find the tubular denting resistance has certain limitations, since the curves are not accurate for minor indentations. Therefore, if dent damage is required to be less than $\frac{w_d}{D} > 0.05$ it follows that the figure cannot be used to verify a design [11]. If the relation between w_d and D is larger than 0.5, the pipeline is assumed to be so damaged that the bending capacity and energy dissipation can be considered exhausted.

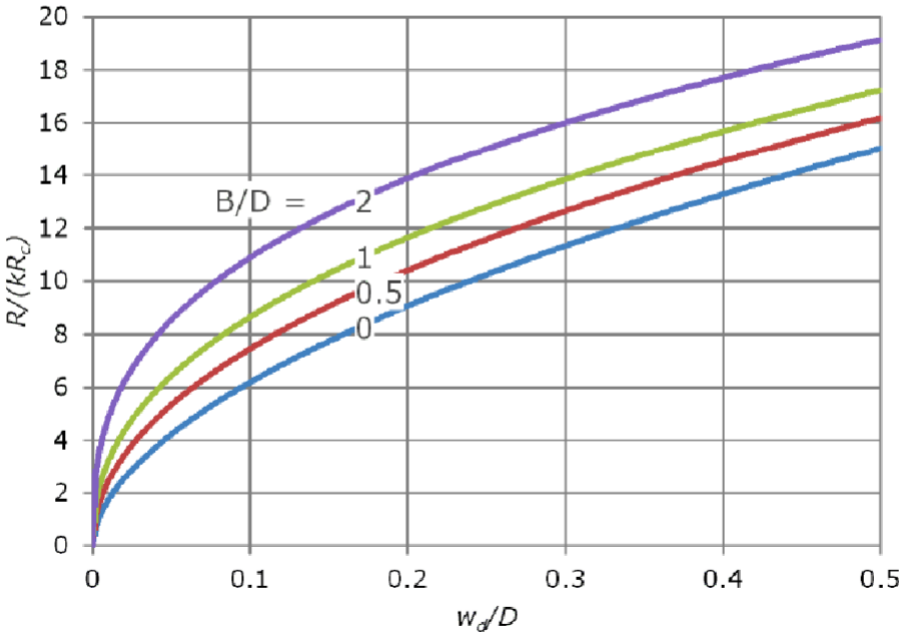

Figure 5 - Resistance curve for local denting [4]

Alternatively, the local denting resistance can be calculated in equation 9 from DNV-RP-C204 [4]:

$$\frac{R}{R_c} = kc_1 \left(\frac{w_d}{D}\right)^{c_2} \tag{9}$$

R_c is the characteristic denting resistance of the tube. The efficiency factor k accounts for the strength reduction due to axial compression loading [4]. The efficiency factor is based on the relationship between the design axial compressive force N_{Sd} and design axial compressive

resistance N_{Rd}. The requirements can be found in DNVGL-RP-C204 section 3.6. To determine the constants c_1 and c_2, the equations 10 and 11 may be used:

$$c_1 = 22 + 1.2\frac{B}{D} \tag{10}$$

$$c_2 = \frac{1.925}{3.5 + \frac{B}{D}} \tag{11}$$

The two constants can be determined based on the relationship between the contact area width and the hit cross-section's diameter.

2.2.6 Damage Classification

The section regarding damage classification can be found in DNVGL-RP-F107 section 4.2 [3]. The damage classifications are typically divided into three levels: minor-, moderate- and major damage. Table 2 shows the damage classifications and typical measurements for the different scenarios.

Table 2 - Damage classification of a structure [3]

Damage level	Measurements
Minor damage (D1)	Damage neither requiring nor resulting in any release of hydrocarbons
Moderate damage (D2)	Damage requiring repair but not leading to a release of hydrocarbons
Major damage (D3)	Damage leading to a release of hydrocarbons or water etc.

2.2.7 Protection Methods

The section regarding protection methods can be found in DNVGL-RP-F107 section 4.6 [3]. To protect a pipeline from external factors such as impacts and corrosion, some type of coating is essential. Examples of protection methods can be seen in Table 3 below.

Table 3 - Other pipeline protection methods [3]

Method	Description	Impact resistance
Concrete blankets	Concrete blankets are well suited for low energy impacts (e.g. trawl board impacts). In general, individual cones of concrete have only limited impact capacity (in the order of 3 kJ), however, several cones may be activated during an impact. Note that the stability of such blankets needs to be confirmed.	5-20 kJ
Sandbags	Sandbags are normally used to build artificial supports. Can be used for protection.	5-10 kJ (assumed)
Bundles	The bundle will act as an effective protection against impact loads. The energy absorption can be calculated as for a bare steel pipe. However, the damage classification will be changed. The only critical failure will normally be leakage. Special attention should be made to towheads and to intermittent bulkheads.	Acc. to equation (3)
Pipe-in-pipe	Similar to bundles. Special attention should be made to intermittent bulkheads.	Acc. to equation (3)
Tunnel structures, nearby protection structures	Tunnel structures are normally introduced in order not to restrain pipeline movements. Tunnel structures can be made up with a variety of geometry and material. Thus, almost any required capacity level can be obtained.	Varies, normally at least 50 kJ
Trenching	Trenching without backfilling will have a positive but limited effect against dropped objects, ships sinking, etc, as these will reduce the possibility to hit the pipeline/umbilical depending on the width of the trench and the size of the impacting object. (i.e. only direct hits will be accounted for)	N.A
Concrete coating	Shielding pipelines for potential impact damage. The crushing strength is from 3 to 5 times the cube strength for normal concrete density.	~ 40 kJ
Polymer coating	Often consists of several layers to protect from different scenarios. Examples are corrosion coating layer, thicker multi-layer coating (insulation) and mechanical protection systems.	0-15kJ
Gravel dump	Protecting a pipeline by burying it in gravel. Used to protect against ship anchors	N.A

This thesis has decided to investigate further the effect of concrete coating. Concrete coating is often used to protect the pipeline from any potential impact damage, due to its high impact resistance of approximately 40 kJ, depending on the concrete quality. This protection method was used for cases 1-6 and 13 (see Table 8) to compare with an unprotected steel pipeline.

3 Methodology

3.1 Finite Element Method

Finite Element Method (FEM), or Finite Element Analysis (FEA), is a technique used to predict an object's behaviour using calculations, models, and simulations. It involves solving numerical problems using differential equations or integral expressions [15]. FEM breaks the object into smaller elements joined at various points called nodes. These elements make up a mesh, and the size of the elements determines the mesh size. The mesh can be represented numerically as algebraic equations that solve unknowns at each node [12].

FEA has several advantages over other numerical analysis methods. It is versatile and can be applied to various field problems, including stress analysis, heat transfer, and magnetic fields. There are no restrictions when it comes to the geometry of the object. Both boundary conditions and different types of loads can be applied wherever wanted. Other material properties can be applied to each element if desired. A Finite Element (FE) model can contain several types of elements within one single model, such as beams, bars and plates. Accuracy can be increased by adjusting mesh size as required [12].

With a smaller mesh size, more accurate results are expected. However, by reducing the mesh size, the computational time will increase. Therefore, finding the optimal mesh size, that generates the desired accuracy with the lowest possible computational time is essential. One way of finding the correct balance between computational time and accuracy is by doing a mesh convergence test. Comparing the same scenario with different mesh sizes can help determine the ideal size. If a mesh refinement has little effect on the results, it can be assumed that the results are converged [13].

The FE code is based on an explicit timestep algorithm for impact analysis. It can simulate the response of materials to short periods of severe loadings [14]. This software can simulate explosions, bird strikes, fractures, drops, impacts and more. For this thesis, dropped tests and impact are the primary concerns.

3.2 Software

3.2.1 LS-DYNA

LS-DYNA is a software developed by Livermore Software Technology Corporation, which was bought by Ansys in 2019 [15]. The software is a pre-and postprocessing tool using general-purpose FEA software. It has many analysis capabilities as well. Some examples are explicit and implicit time integration, linear and non-linear statics, non-linear dynamics and large deformations [15]. According to Ansys, LS-DYNA is the industry-leading explicit simulation software application for drop tests, impact and penetration, smashes and crashes, among others [14].

LS-PrePost is a pre-and postprocessor used to make models based on input data, and analyse LS-Run results. It is also the tool for importing, editing and exporting LS-DYNA keyword files and making input files [16].

LS-Run runs simulations from LS-PrePost using an SMP or MPP version of LS-DYNA with single (explicit) or double (implicit) analysis. The explicit time integration is more memory efficient and is suitable for dynamic problems such as impact and shock simulations. The implicit analysis uses more memory. It is suited for static and quasi-static issues and eigenmode-based linear dynamics [16]. For more extensive analyses, simulations in this program can be very time-consuming. Therefore, a good option can be to use High-Performance Computing (HPC) instead.

3.2.2 High-Performance Computing

HPC processes large amounts of data quickly to get faster results than a laptop. One example of HPC is a supercomputer. A supercomputer is made of several smaller computers and their processors. This is also called an HPC cluster, where hundreds of thousands of computer servers are networked. Each of these servers is called a node. These nodes work together, which leads to an increase in processing speed [17]. The nodes talk to each other through a communications network [18]. The network used in this thesis is called FRAM.

FRAM is a cluster network located at the University of Tromsø (UiT), the Arctic University of Norway. It is a distributed memory system with 1004 dual sockets and two quad socket nodes connected to a high-bandwidth, low-latency Infiniband network [19].

4 Finite Element Model

4.1 Container Model

The container model was designed by Aker Solutions, and imported into the model used for the analysis. They have designed the container based on a 20-ft standard shipping container. The container has a length of 5.97m, a width of 2.43m and a depth of 2.82m. It consists of top and bottom rails, corner posts and fitting, and longitudinal and transverse beams. The whole model has been designed using shell elements [20].

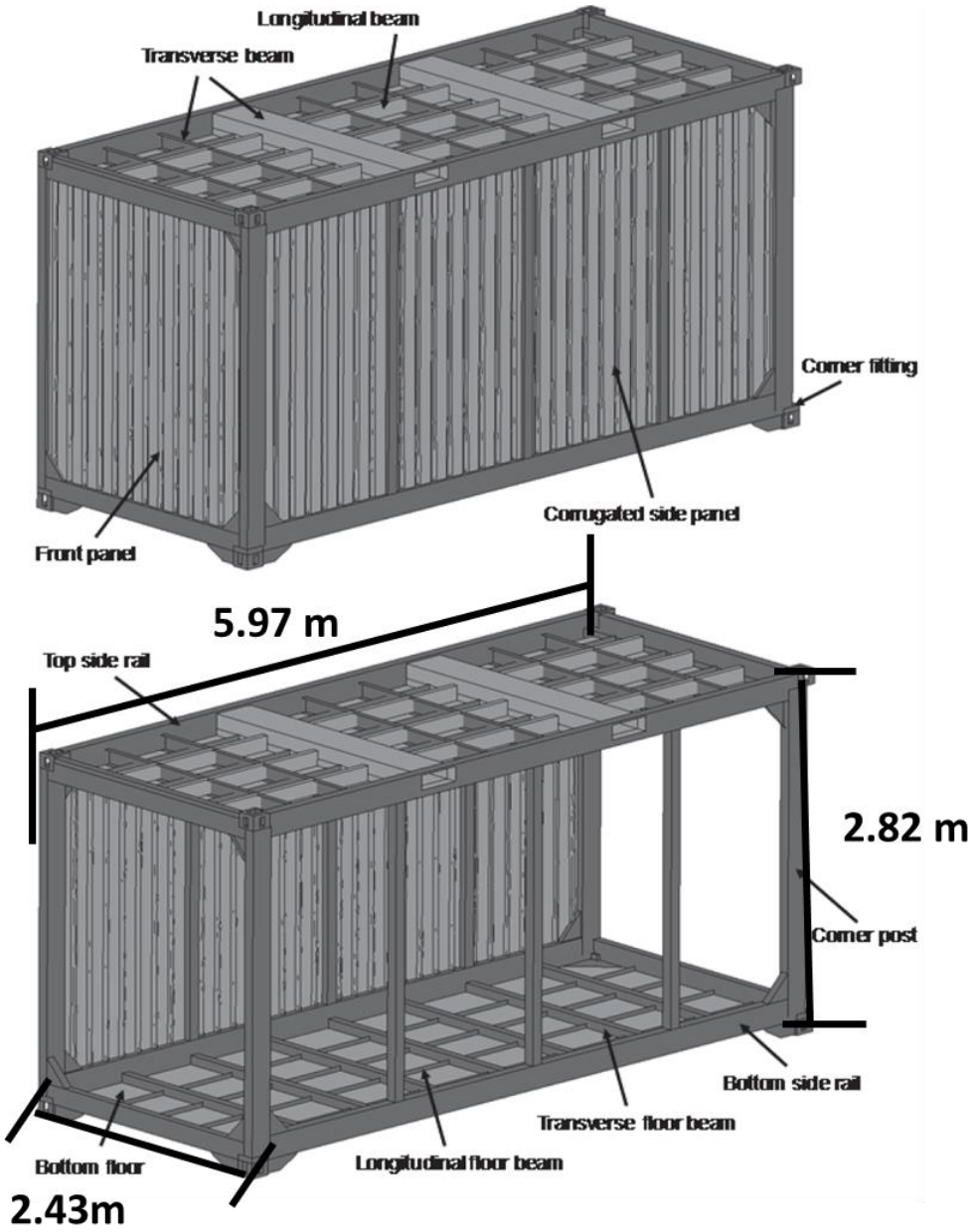

Figure 6 - Modelled container [20]

4.2 Pipeline

Two different pipelines have been modelled using solid elements. One pipeline was modelled with a concrete coating to protect the steel pipeline, and the other was modelled as a steel pipeline without protection. A perfect transition between the steel and concrete is assumed. No steel reinforcement has been used in the concrete coating. Both the steel pipeline and the concrete coating have a thickness of 50 mm. The steel pipeline has an inner radius of 450 mm, and the concrete has 550 mm. The length of the pipelines is 6 m.

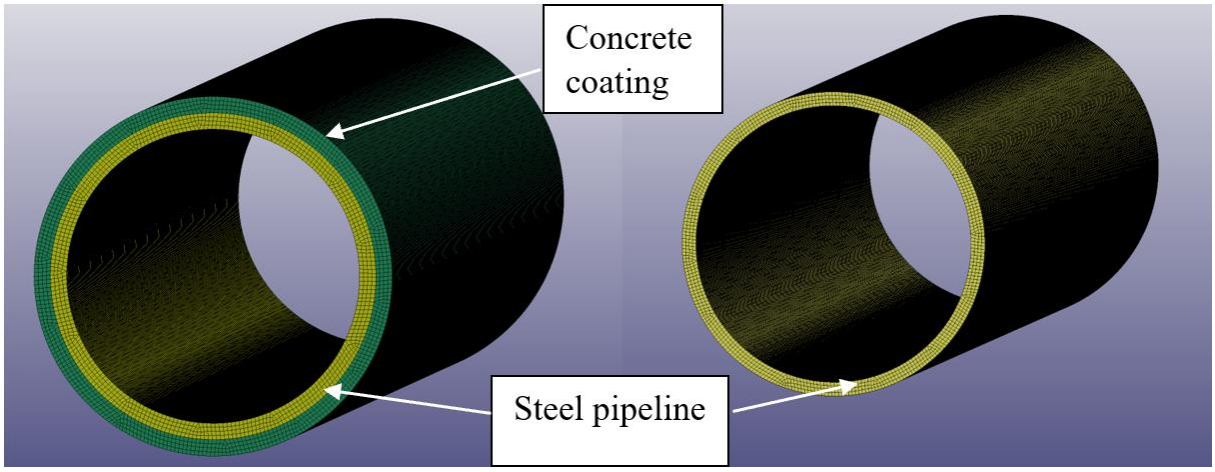

Figure 7 - Modelled pipelines [21]

4.3 Seabed

The seabed has also been modelled using solid elements. The model has a length of 6 meters, width of 2 meters and a depth of 1 meter. The rigid seabed is not modelled. Instead, boundary conditions have been applied to the pipeline, simulating a rigid seabed.

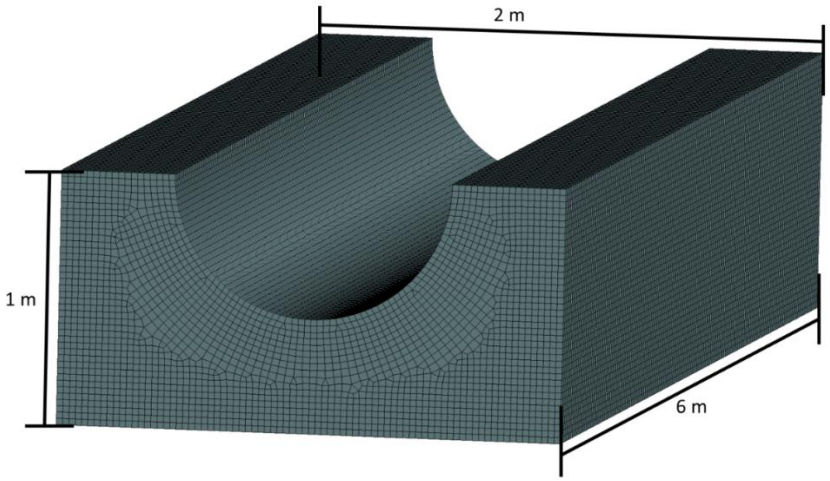

Figure 8 - Modelled flexible seabed [21]

4.4 Geometry of the Model

The pipeline, seabed and container have the following geometry:

Table 4 - Geometry of the Model

	Inner radius [m]	**Outer radius [m]**	**Thickness [m]**
Steel pipeline	0.45	0.50	0.05
Concrete coating	0.50	0.55	0.05
	Length [m]	**Width [m]**	**Depth [m]**
Seabed	6	2	1
Container	5.97	2.43	2.82

4.5 Material

The choice of material property is important to decide the material behaviour in different situations. In the model, three different materials have been used. The materials used are LS-DYNA numbers 24, 14 and 159, described in Chapters 4.5.1, 4.5.2 and 4.5.3.

4.5.1 Piecewise Linear Plasticity

Piecewise Linear plasticity (material number 24 in LS-DYNA) was chosen for the steel part of the pipeline. Two different steel material grades have been used for the pipeline. Steel grade S275 has been used for cases 1-12 (see Table 8). S355 was used in case 13 (see Table 8). The material is an elastoplastic material model for a material undergoing plastic deformation. One advantage of the material is that it can define an arbitrary stress-strain curve and strain rate dependency, leading to more accurate results. This is because it is possible to define up to eight stress and strain points, to define a more realistic stress-strain behaviour. The different stress and strain points can be found in Tables 10 and 11. The stress-strain curve for both material grades is shown in Figure 9 below [22].

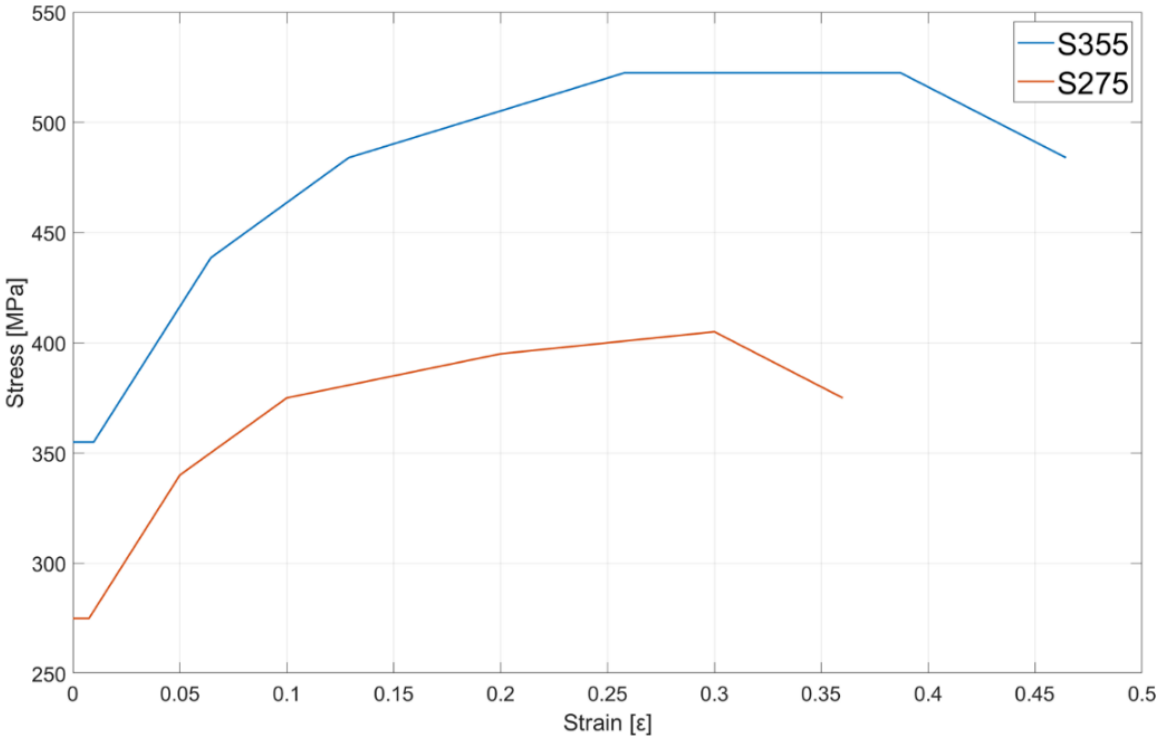

Figure 9 - Stress-strain curve of the two steel grades

4.5.2 Mat Soil and Foam Failure

The Mat Soil and Foam Failure (material number 14 in LS-DYNA) was used for the model's seabed. The material was developed by Krieg in 1972 [23]. It is suitable for cohesionless soils, like sand. It can detect a failed element by defining a failure pressure. A seabed consisting of loose sand was compared to a rigid seabed using this material property.

The material properties have been decided based on the article "Finite element method simulation of explosive compaction in saturated loose sandy soils" written by M. Esmaeili and B. Tavakoli [23]. The material property can be seen in Table 5 below.

Table 5 - Material property number 14 [23]

*MAT_SOIL_AND_FOAM_FAILURE_(TITLE) (1)

	TITLE							
	Seabed1							
1	MID	RO	G	BULK	A0	A1	A2	PC
	201	1700.0000	2.524e+006	4.673e+009	1.000e+009	4900.0000	0.0079000	-5.000e+004
2	VCR	REF						
	0.0	0.0						
3	EPS1	EPS2	EPS3	EPS4	EPS5	EPS6	EPS7	EPS8
	0.0	-0.0216000	-0.0437000	-0.0895000	-0.1374000	-0.1878000	-0.2408000	-0.5586000
4	EPS9	EPS10						
	-1.0272000	-1.9380000						
5	P1	P2	P3	P4	P5	P6	P7	P8
	0.0	1.000e+008	2.000e+008	4.000e+008	6.000e+008	8.000e+008	1.000e+009	2.000e+009
6	P9	P10						
	3.000e+009	4.000e+009						

4.5.3 Concrete Surface Cap Model

The Concrete Surface Cap Model (CSCM) (number 159 in LS-DYNA) was developed in the 1990s by US Department of Transportation Federal Highway Administration [24]. It was first designed to simulate the deformation and failure of concrete roadside structures impacted by vehicles. The material features isotropic constitutive equations, three stress-invariant yield surfaces with translation for pre-peak hardening, a hardening cap that expands and contracts, damage-based softening with erosion and modulus reduction, and rate effects for increasing strength in high-strain rate applications.

There are some limitations to using CSCM. It has no direct measurement of the softening behaviour (fracture energy) in pure shear stress. The fracture energy can be described as the area under the stress-displacement curve. The information regarding rate effects is limited to only providing information on the uniaxial tensile and compression stress [24].

The material was mainly developed to simulate the deformation and failure of concrete roadside structures impacted by a vehicle. Since this thesis also assesses an impact, the CSCM has been chosen for the concrete coating. Table 6 below shows the model properties used for the coating.

Table 6 - Material property number 159 [24]

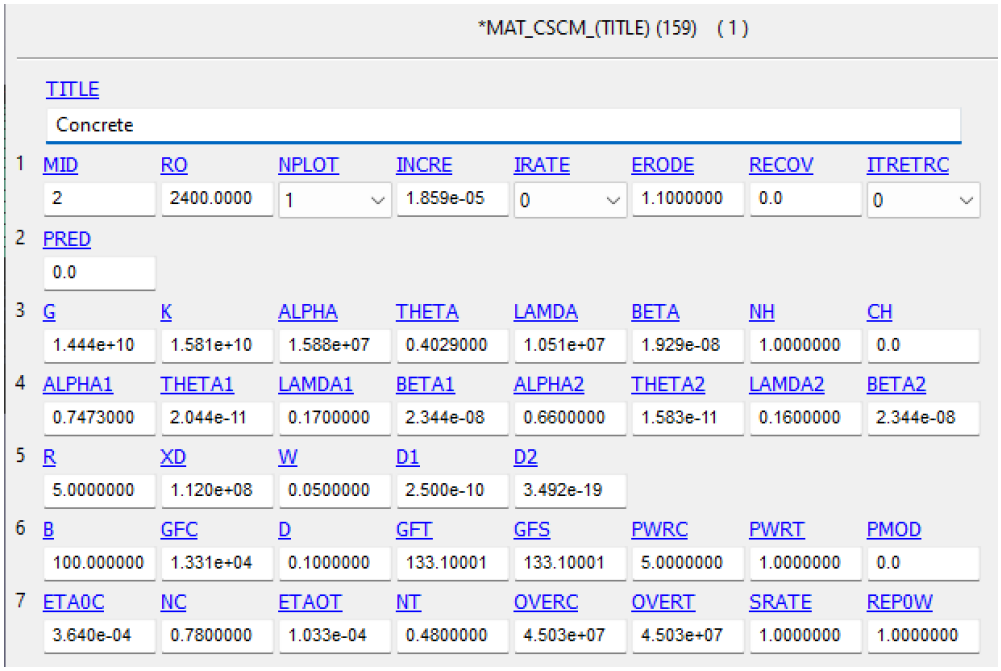

4.6 Initial Velocity

The initial velocity is a keyword in LS-DYNA used to apply a velocity to an object. The velocity can be applied in both translational and rotational directions. In this case, the velocity has been applied to the container in the translational Z-direction, with a constant value of 10 m/s. Since the initial velocity of the container is constant for all impact scenarios, the exact value of the velocity does not affect the results of the comparison.

Table 7 - Initial Velocity [21]

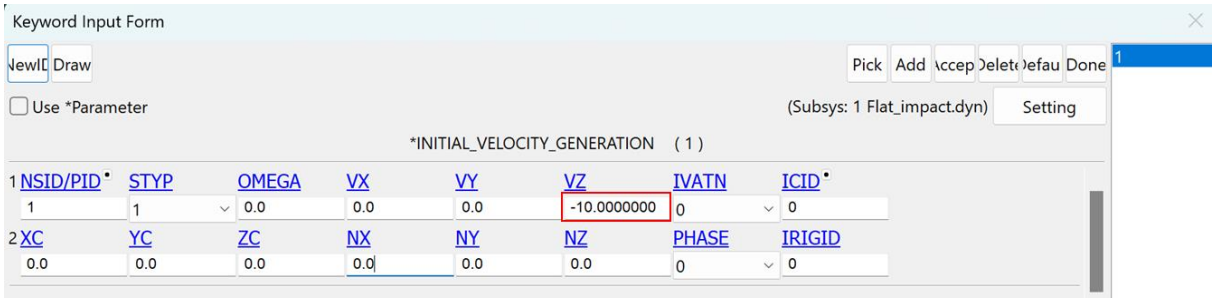

4.7 Contact

Contacts have been defined between the pipeline and the container, and between the pipeline and the seabed. The contact defines one part as a slave element and one as a master element.

Each slave node will then be checked for penetration through the master nodes. After a penetration is found, a force corresponding to the penetration depth is applied to resist the penetration. This is called a penalty-based contact. Different contact types may be used for different situations [25]. In this model, the keyword *contact_automatic_surface_to_surface* is used. This keyword is recommended for crash analyses since it is hard to predict the orientation of the parts when objects undergo large deformations. The automatic contact also checks for penetration on either side of the element [25].

4.8 Boundary Conditions

Boundary Conditions (BC) are constraints necessary to define how a structure interacts with surrounding elements [26]. An example can be to put boundary conditions on a wall structure, constrained in all directions, to simulate how a wall can be connected to the ground.

All models use nodal BC with the keyword BOUNDARY_SPC. SPC is short for single point constraints and defines constraints on selected nodes in the model [27]. The BC nodes have been constrained in both translational and rotational directions.

Figure 10 shows how the BC has been applied for the scenarios with a flexible seabed. Figure 11 shows how the BC has been applied on the lower part of the pipeline for the rigid seabed scenarios. The BC are shown as small black dots.

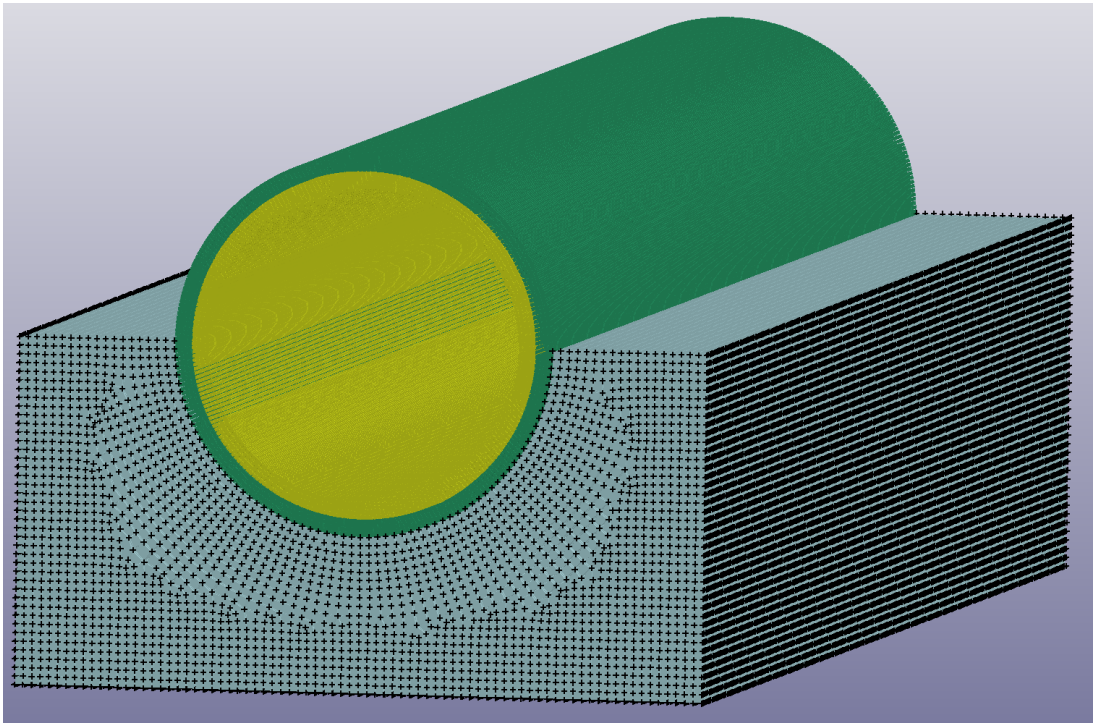

Figure 10 - BC around the flexible seabed [21]

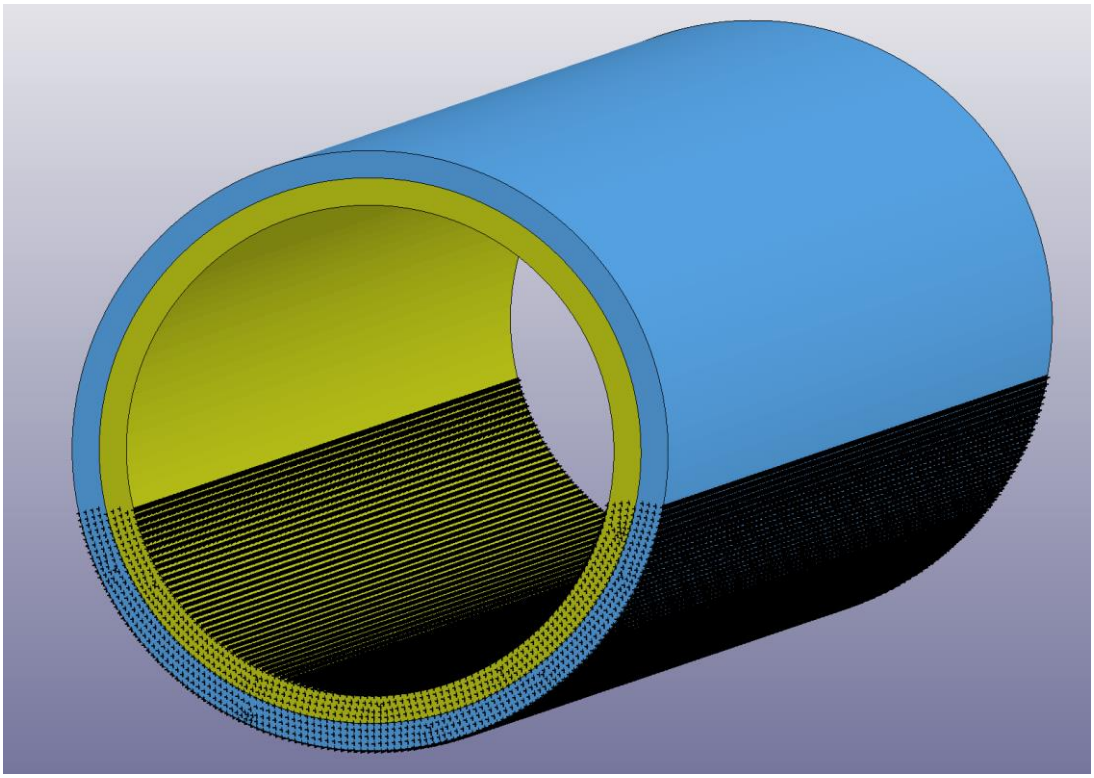

Figure 11 - BC on the rigid pipeline [21]

4.9 Element Type

4.9.1 Solid

Solid elements represent the structure as a through-thickness component with a solid character in all dimensions. Figure 12 shows an example of a solid element, which shows the elements with a through-thickness character. The mesh is on the surface and through the structure [30].

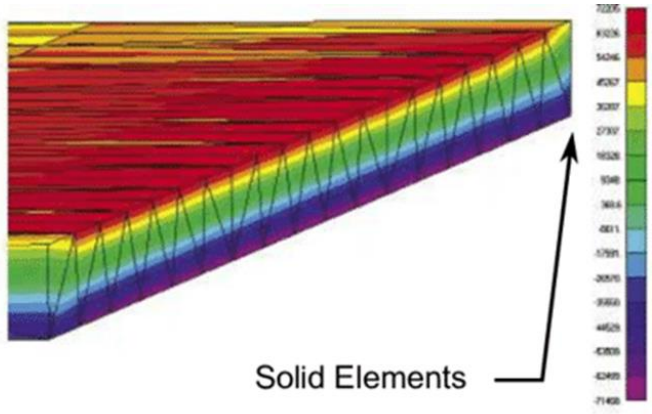

Figure 12 - Solid element [28]

4.9.2 Shell

Shell elements are hollow inside the structure and only model the outer shell. It is a simplification of a solid element. Thin shell elements are only 2D and use the third dimension as thickness in property tables. One of the advantages of using shell elements is that it reduces the computational time, compared to using solid elements. This is because it has fewer mesh elements. Thin shell elements do not consider stresses in the direction perpendicular to the shell surface [29]. Figure 13 shows the same model as for the solid element, only modelled as a shell element, without thickness.

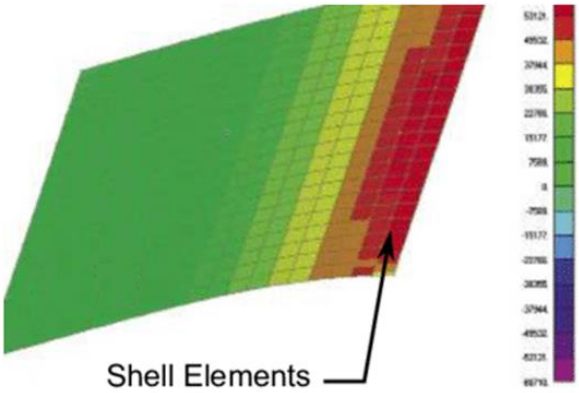

Figure 13 - Shell element [28]

4.10 Mesh Size

In a Finite Element Analysis (FEA) program, meshing is vital to run a simulation accurately. A mesh is a collection of nodes representing the object's shape. With more nodes, you get a finer mesh and a more accurate object representation. This leads to a better result than a coarser mesh [30].

There are, in general, two main types of mesh, tetrahedral and hexahedral mesh. As seen in Figure 14, a hexahedral mesh type typically has four sides and is more accurate for fine meshes than tetrahedral elements. If the geometry is more advanced, tetrahedral can be a better choice [30].

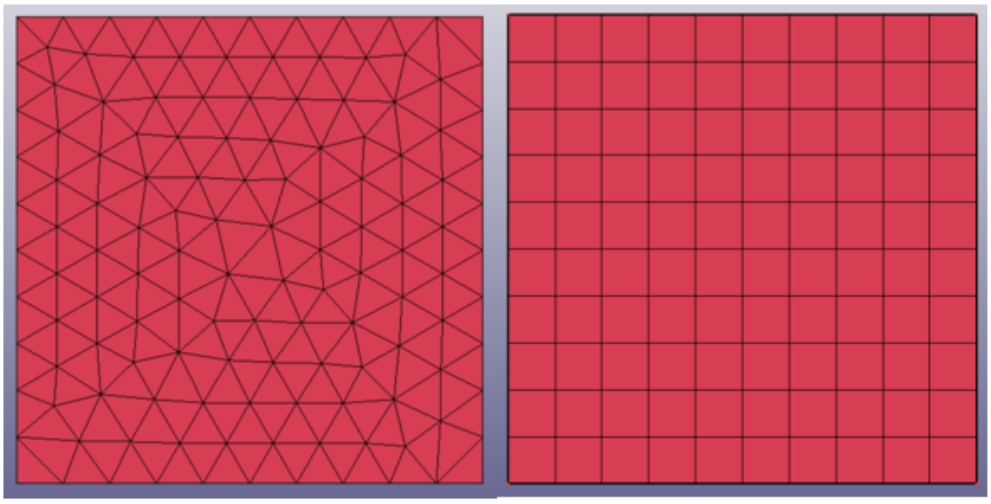

Figure 14- Tetrahedral mesh to the left and hexahedral mesh to the right [21]

A good mesh leads to more accurate results but is more time-consuming and uses more of the computer's memory. Therefore, the mesh has been divided into coarse and fine sizes, as seen in Figure 15. The coarse mesh has a mesh size of 25 mm and was used for the seabed to reduce the computational time. The fine mesh has a mesh size of 12.5 mm and was used for the pipeline.

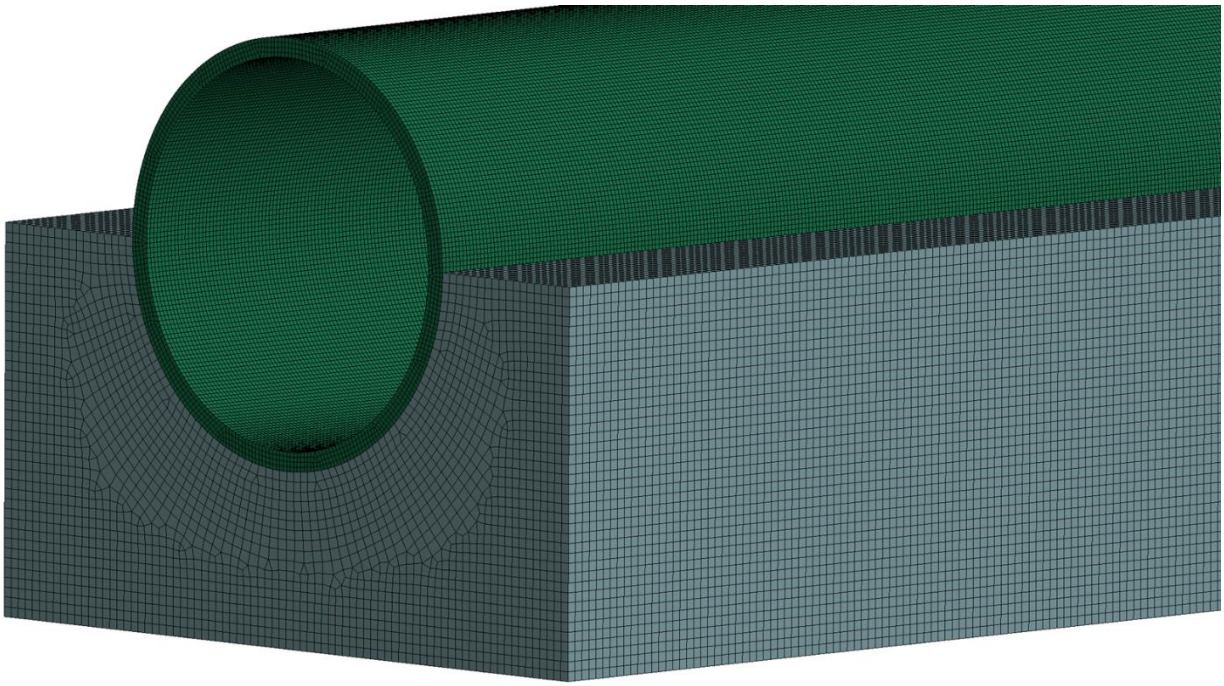

Figure 15 - Fine and coarse mesh of the pipe and soil [21]

4.11 Impact Scenarios

Thirteen impact scenarios have been compared in addition to three cases used in a convergence test. Impact scenarios 1-3 and 7-9 have been modelled with a flexible seabed, while scenarios 4-6 and 10-13 are modelled with a rigid seabed. Scenarios 1-6 and 13 were modelled with a pipeline protected by concrete coating. Scenarios 7- 12 were modelled with an unprotected pipeline. Since the dropped object would move in water, it was difficult to determine at what angle the container would hit the pipeline. It was decided to test all scenarios with the three container impact angles assumed to be the most critical. The angles tested were flat, side and tip impact. Scenarios 1-12 have a yield strength of 275 MPa, and scenario 13 has a yield strength of 355 MPa. Impact scenarios 1-3 and 7-9 can be seen in Figure 16, and scenarios 4-6 and 10-13 in Figure 17. Table 8 shows the 13 cases and what each scenario includes. Scenarios 14-16 in Table 9 have been used for a convergence test.

Table 8 - Impact scenarios modelled in this thesis

Case Number	Seabed	Coating	Impact Angle	Pipeline steel grade
1	Flexible	Yes	Flat	S275
2	Flexible	Yes	Side	S275
3	Flexible	Yes	Tip	S275
4	Rigid	Yes	Flat	S275
5	Rigid	Yes	Side	S275
6	Rigid	Yes	Tip	S275
7	Flexible	No	Flat	S275
8	Flexible	No	Side	S275
9	Flexible	No	Tip	S275
10	Rigid	No	Flat	S275
11	Rigid	No	Side	S275
12	Rigid	No	Tip	S275
13	Rigid	Yes	Tip	S355

Table 9 - Impact scenarios for convergence test

Case number	Container	Pipeline	Mesh size [mm]
14	Rigid	Deformable	6.25
15	Rigid	Deformable	12.5
16	Rigid	Deformable	25

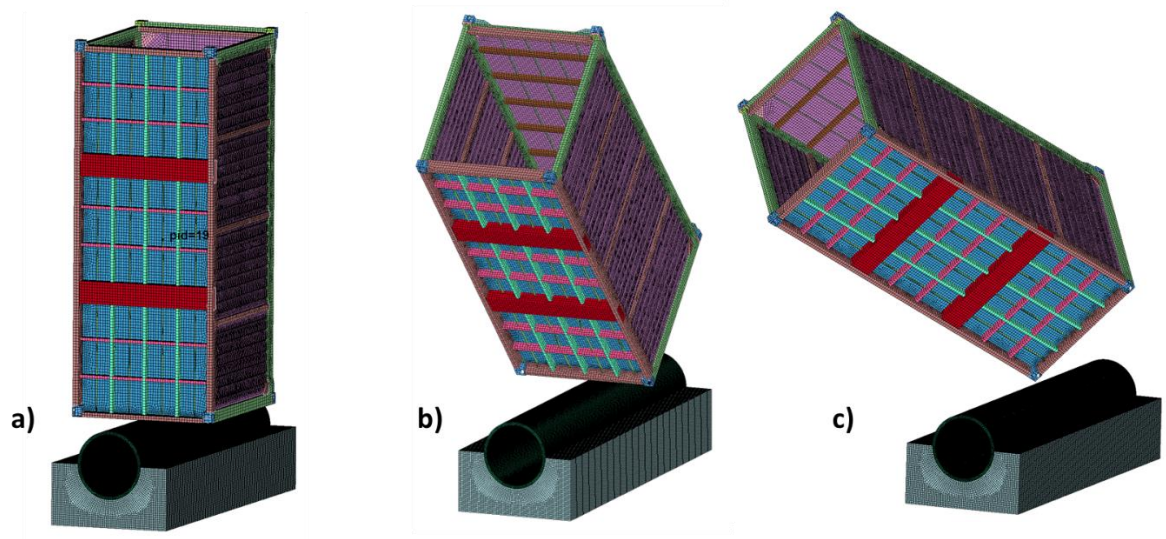

Figure 16 - a) Flat impact, b) Side impact, c) Tip impact, (For case numbers 1-3 and 7-9) [21]

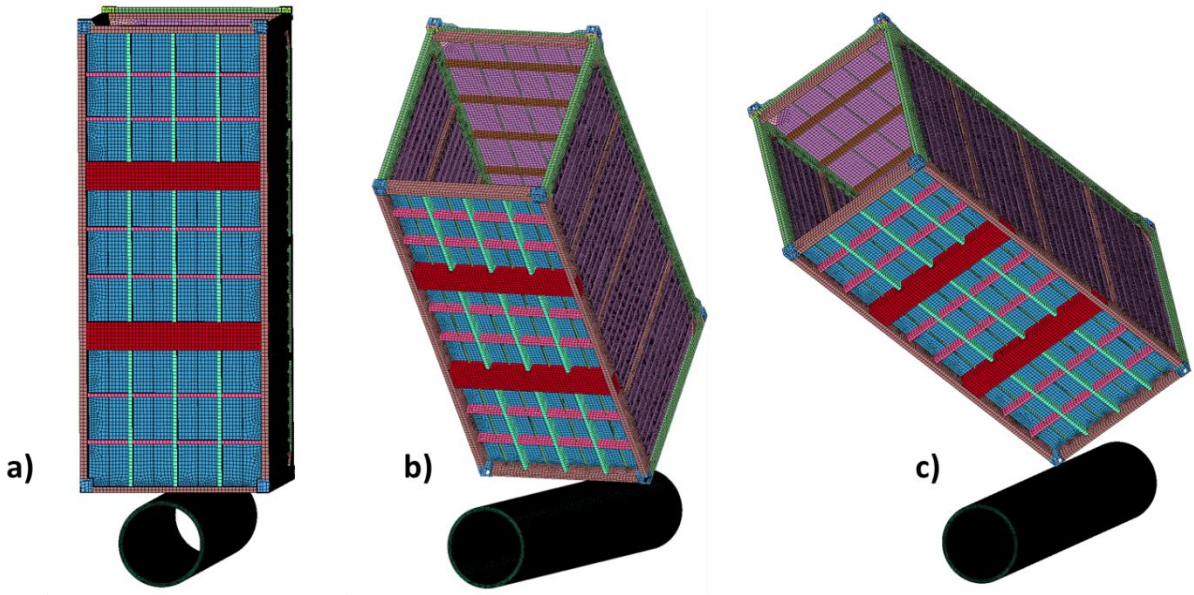

Figure 17 - a) Flat impact, b) Side impact, c) Tip impact, (For case numbers 4-6 and 10-13) [21]

5 Numerical Results and Discussions

5.1 Convergence Test

The convergence test checked a simplified model with three different mesh sizes. The scope of this test was to reduce computational time as much as possible by using the largest possible mesh size without sacrificing the accuracy of the results. Therefore, it was tested for three mesh sizes, 6.25 mm, 12.5 mm and 25 mm.

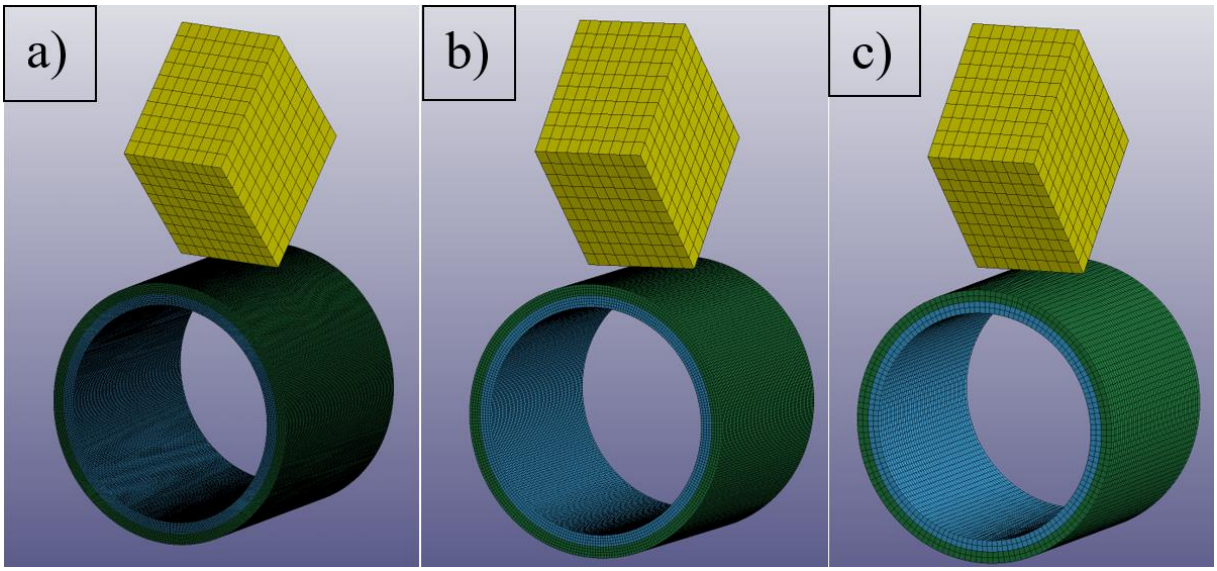

Figure 18 - a) 6.25 mm mesh, b) 12.5 mm mesh, c) 25 mm mesh, (cases 14-16) [21]

The simplified model used a rigid container model and a deformable pipe. The results have been compared for internal energy, impact force and deformation, to determine which mesh size was necessary to get the desired accuracy.

5.1.1 Deformation

Node number 26435581 has been used for scenarios 14-16. The selected node is located on the top part of the steel pipeline (see Figure 19).

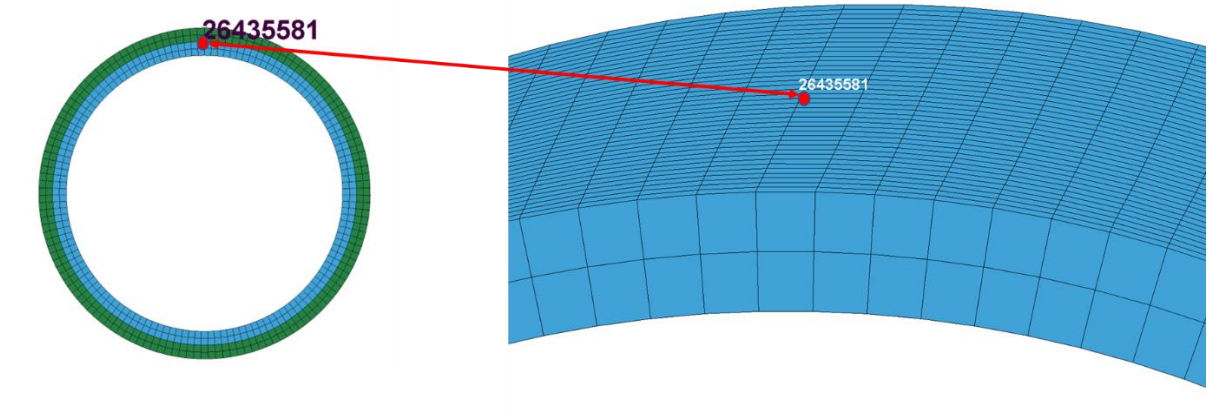

Figure 19 - Node position used to determine deformation of the pipelines [21]

The 6.25 mm mesh was expected to be the most accurate since it had the highest number of elements. A cut in the graph has been made to see the difference between the three mesh sizes and compare (see Figure 20). The results show that the 6.25 mm and the 12.5 mm mesh follow a similar path. This does not occur for the 25 mm mesh. This suggests that the 25 mm mesh does not converge as well as mesh sizes 6.25 mm and 12.5 mm.

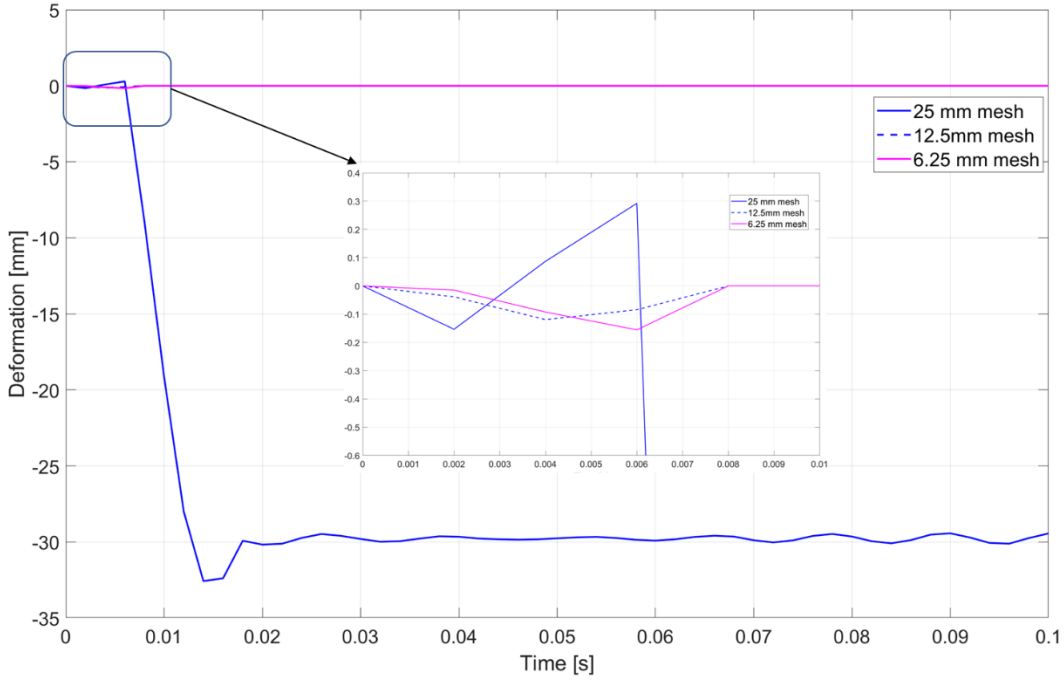

Figure 20 - Deformation of node 26435581 (for scenarios 14-16)

5.1.2 Internal Energy

The internal energy convergence test also confirms that the 12.5 mm mesh was closer to the 6.25 mm mesh than the 25 mm mesh was to the 6.25 mm mesh. It was hard to know in advance which mesh size would give the highest and lowest internal energy. However, the expectation was that the smaller the mesh size, the more accurate and more converged the results would be. For the internal energy convergence test, this was correct. Using the 6.25 mm mesh as a guide for what was expected to be the correct value, one can see that the 25 mm mesh had a larger deviation compared to the 12.5 mm mesh and was, therefore, less converged.

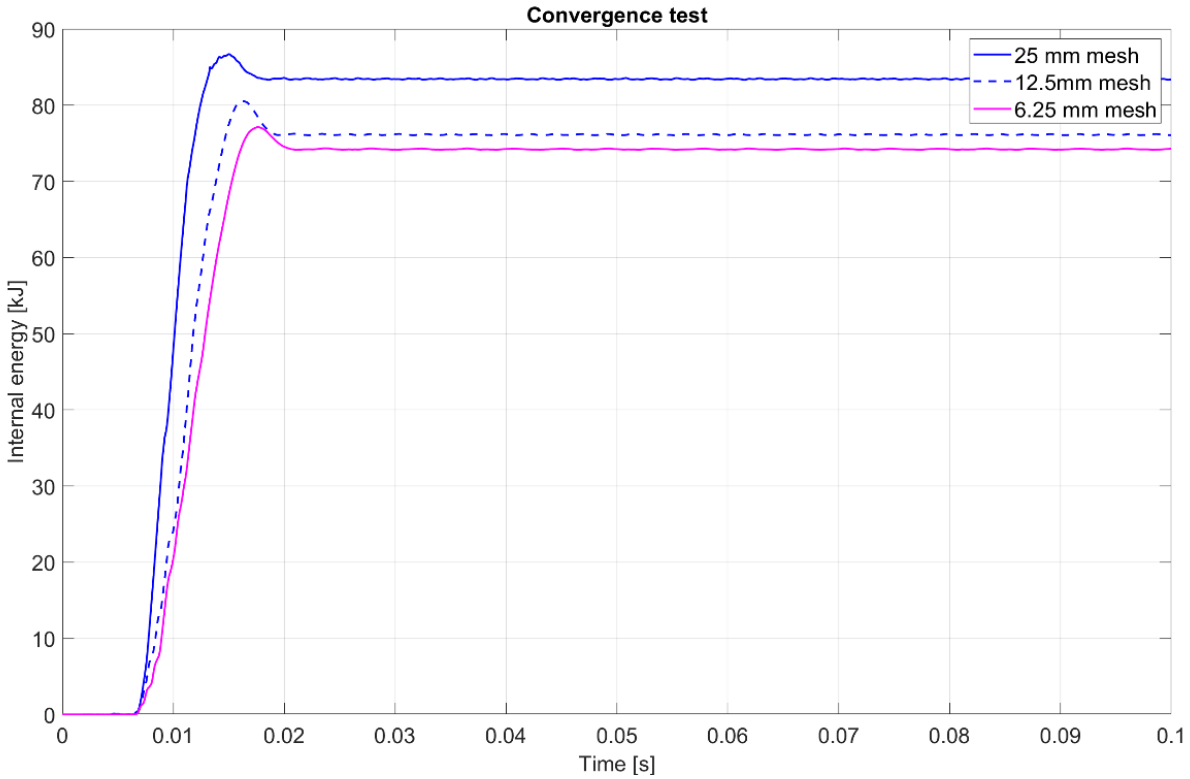

Figure 21 - Internal energy of pipeline (cases 14-16)

5.1.3 Impact Force

Figure 22 shows the impact force from the container on the pipeline with respect to time. Using the 6.25 mm mesh as a guide, the 25 mm mesh was found to deviate significantly. The 12.5 mm mesh follows the guideline more closely, with some minor exceptions. These results show more significant deviations between the different mesh sizes compared to internal energy, suggesting that the mesh sizes 12.5 mm and 25 mm were not fully converged.

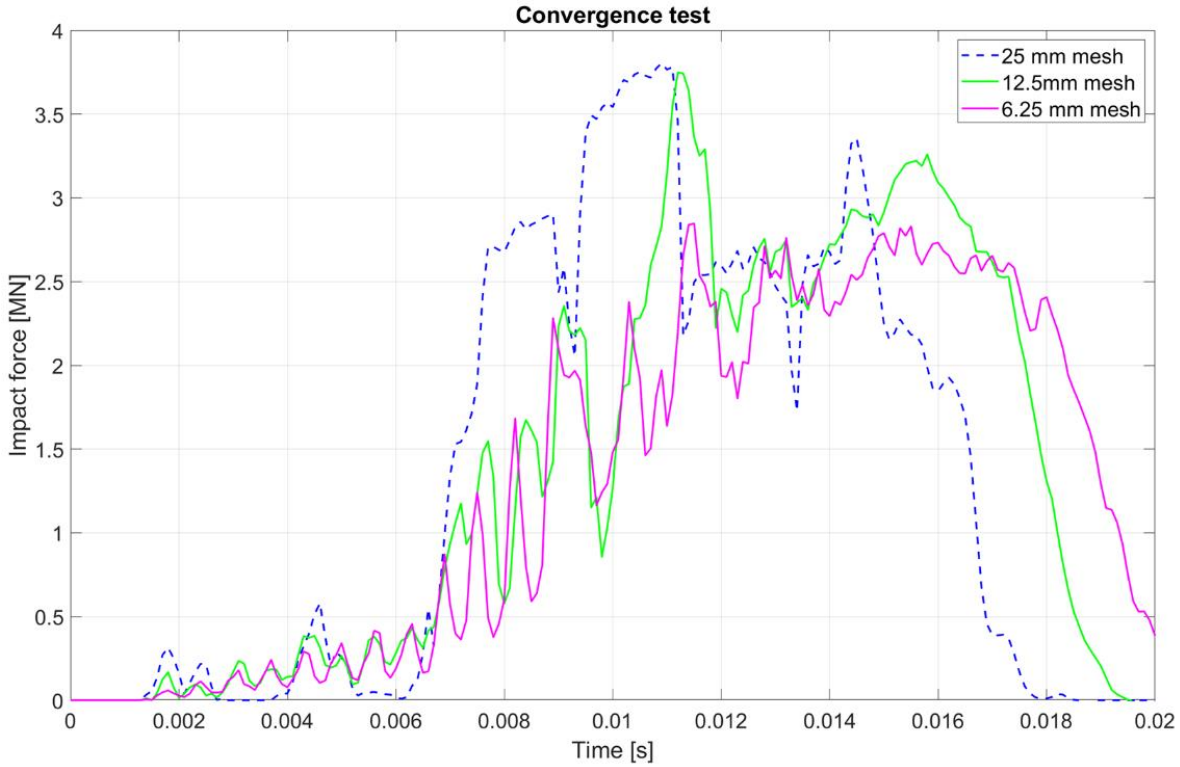

Figure 22 - Impact force on the pipeline (cases 14-16)

5.1.4 Mesh Size

Which mesh size to use has been decided based on the results in Chapters 5.1.1, 5.1.2 and 5.1.3, and the amount of computational memory available. The deformation shows some apparent differences with different mesh sizes. The internal energy and impact force shows some deviation between the 25 mm and 6.25 mm mesh. The 12.5 mm mesh was closer to the 6.25 mm mesh. There are still some differences between the 12.5- and 6.25 mm mesh, so the optimal choice would be the 6.25 mm mesh. However, when using a 6.25 mm mesh, the computational time increased significantly. Balancing these two parameters, a decision was made to accept the results from the 12.5 mm mesh as sufficient for this model.

5.2 Impact Force

The impact forces have been compared with and without pipeline coating, with three different impact points, and also with the effect of flexible vs rigid seabed taken into consideration. Impact scenarios used in this analysis are cases 4-6, 8 and 10-12. The tip impact was expected to damage the pipeline the most and create the largest impact force. The hit surface will be small, resulting in easier pipeline penetration. A steel pipeline without protection was expected to suffer more damage than a pipeline with a protective coating. Likewise, a model with a rigid

seabed would cause more damage to the pipeline, as no impact energy is absorbed by the surroundings. A flexible seabed was expected to help reduce the impact on the pipeline, reducing the total damage.

5.2.1 With Coating

Impact scenarios 4-6 have been used in this comparison. The curve for flat impact had the second-highest peak impact force. It had a more even curve with smaller force changes than the tip impact. This was because the flat impact had a more significant impact area, destroying less coating. Therefore, the container would be deformed, and there would be less damage to the pipeline.

The tip impact had more peaks and drops in values. This was because elements were deleted when the container destroyed them, lowering the impact force before it increased when hitting the next element. This is called a penalty-based contact, explained in Chapter 4.7 regarding contacts. A typical example is shown in Figure 23 below. Since the tip impact destroyed the concrete, more of the deformation would be in the pipeline, resulting in less damage and deformation to the container than with the flat impact.

The side impact was more of a mix between the flat and tip impact. It had the lowest impact force of the three, with minimal differences between the peak and the next drop. This indicated that the container took most of the damage in this scenario.

The results confirmed that previous assumptions were correct, where the tip impact looked to be the scenario damaging the pipeline the most.

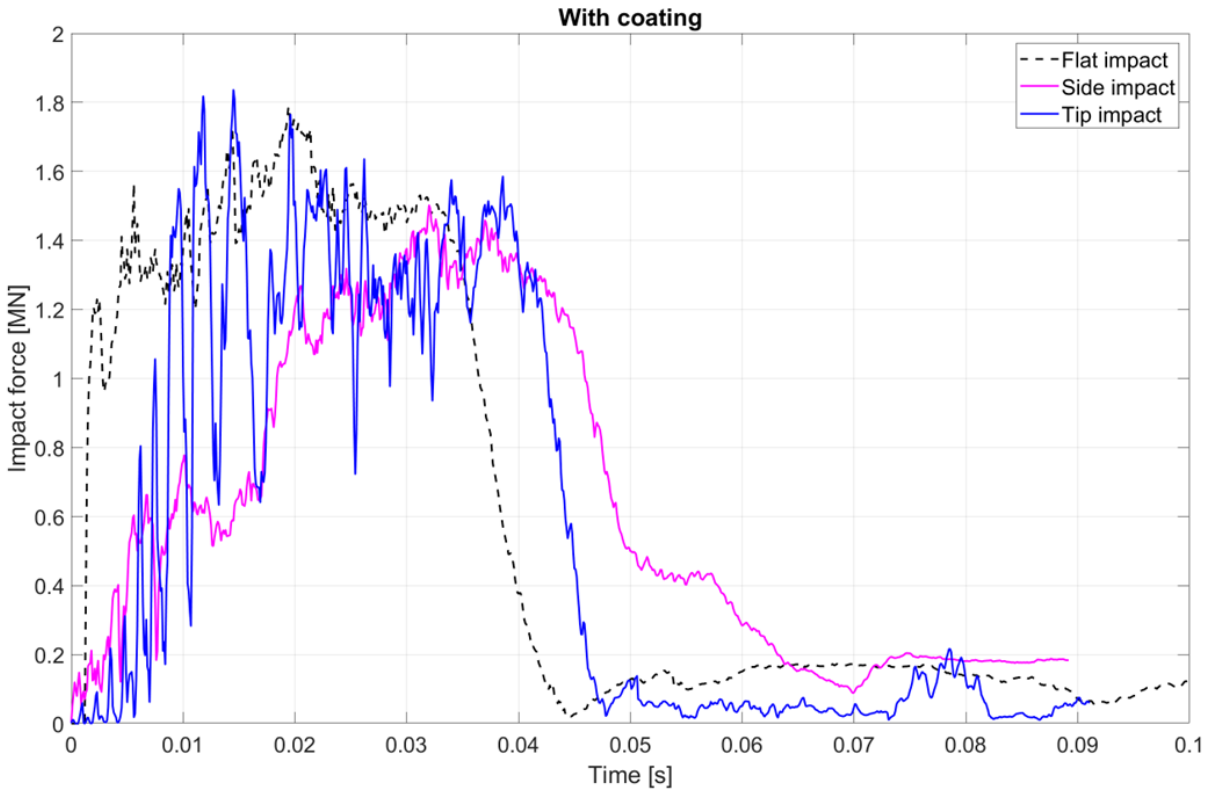

Figure 23 - Impact force with coating

5.2.2 Without Coating

Impact scenarios 10-12 have been used in this comparison. As explained for the models with coating, considerable differences between the peaks and the subsequent dip indicate damage to the pipeline.

There were a few peaks for the flat impact followed by big dips. This indicated that it might be some slight damage to the pipeline, but it looked like there was also some damage to the container. The tip impact had very clear peaks and dips, indicating that most of the damage was done to the pipeline. It looked, in general, very similar to the result with coating protection. The side impact had no prominent peaks followed by a dip, indicating that most damage was done to the container, not the pipeline. It also had a lower and more even force curve.

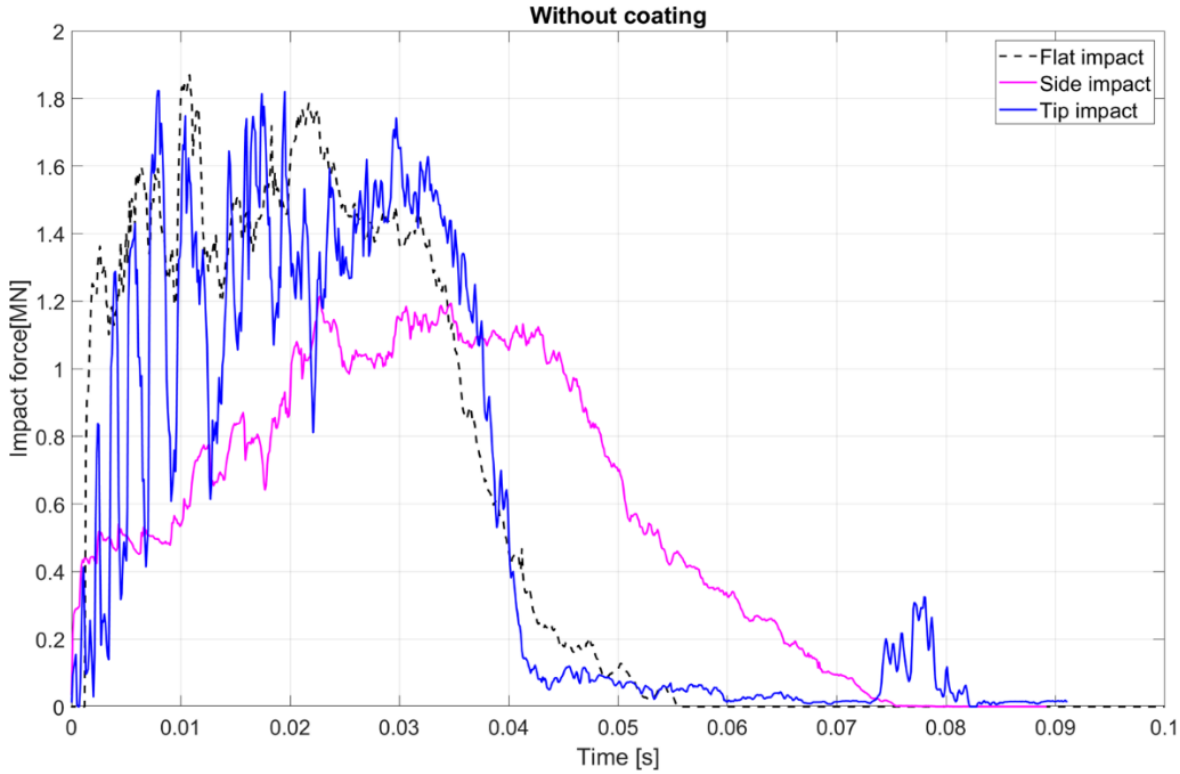

Figure 24 - Impact force without coating

The flat impact acts similarly both in the scenario with and without coating. The scenario without coating had a peak value of right above 1.8 MN, while the scenario with coating had a peak value of right below 1.8 MN. The side impact showed a higher and steeper graph for the scenario with coating protection. The differences in peaks and dips indicated that the container was crushing some of the coatings. This was because the concrete is less elastic than the steel and would therefore be destroyed by the impact. The graphs for the model without coating were slightly lower and more even than those with coating. This could be due to the elastic steel pipeline dampening the container's impact, resulting in a lower impact force. The scenarios for tip impact looked very similar for both with and without coating protection.

5.2.3 Flexible vs Rigid seabed

Impact scenarios 8 and 11 have been used in this comparison. Figure 25 compares impact force between a side impact scenario with a flexible seabed and one with a rigid seabed. The graphs are almost identical, with only slight variations compared to each other. It was not expected to be much difference in these results since there was no change in the container's velocity, mass, or impact position.

Previous research by M. R. U. Kawsar et al. [9] have been conducted considering the effect of the seabed's flexibility. As expected, the article concluded that a model with a rigid seabed would be more prone to damage from an impact compared to a flexible seabed.

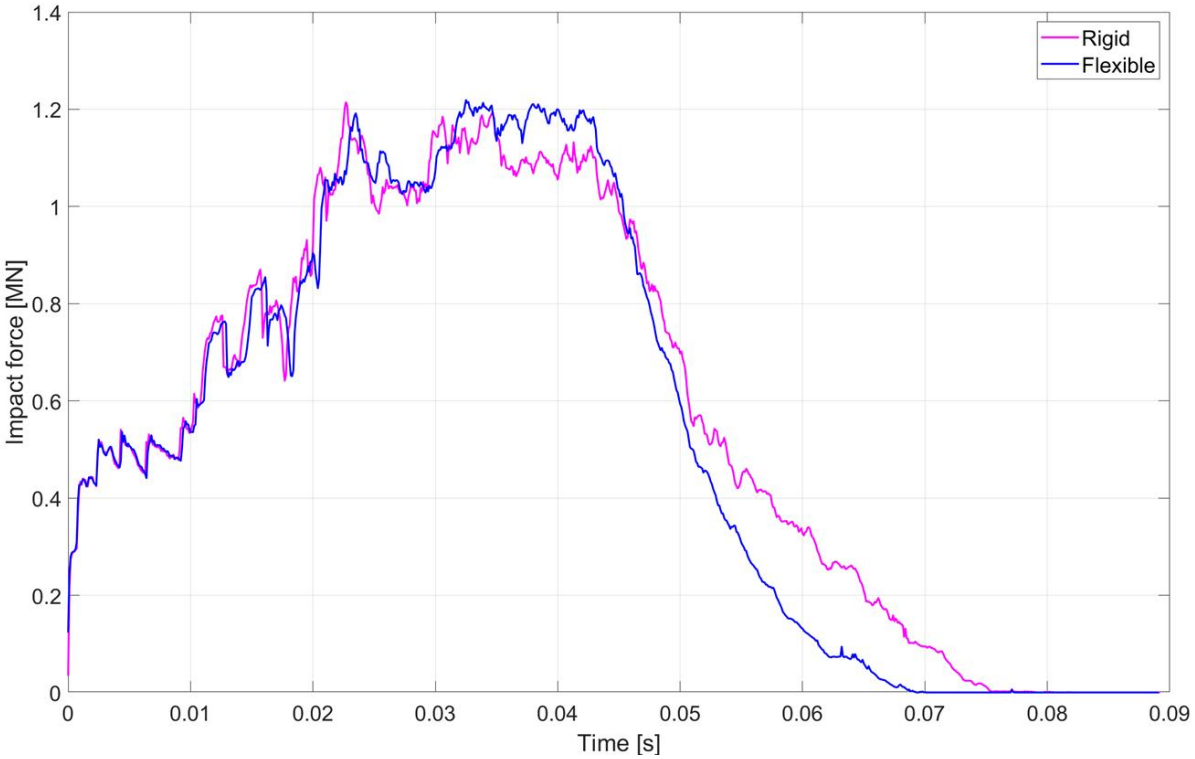

Figure 25 – Effect of rigid and flexible seabed

5.3 Deformation

Impact scenarios 4-6, 8 and 10-12 have been used when comparing the deformation of the pipeline. The deformation has been tested for the same node for all scenarios. The node selected was node number 13211421 (see Figure 26 below). It is located on the outer layer of the steel part of the pipeline. The deformation was expected to be most significant for the tip impact. The container will transmit all its energy through a small hit surface, resulting in a bigger deformation. A. Ramberg's research [6] supports these assumptions. With a bigger impact area, more energy was absorbed by the container, resulting in a lower pipeline deformation.

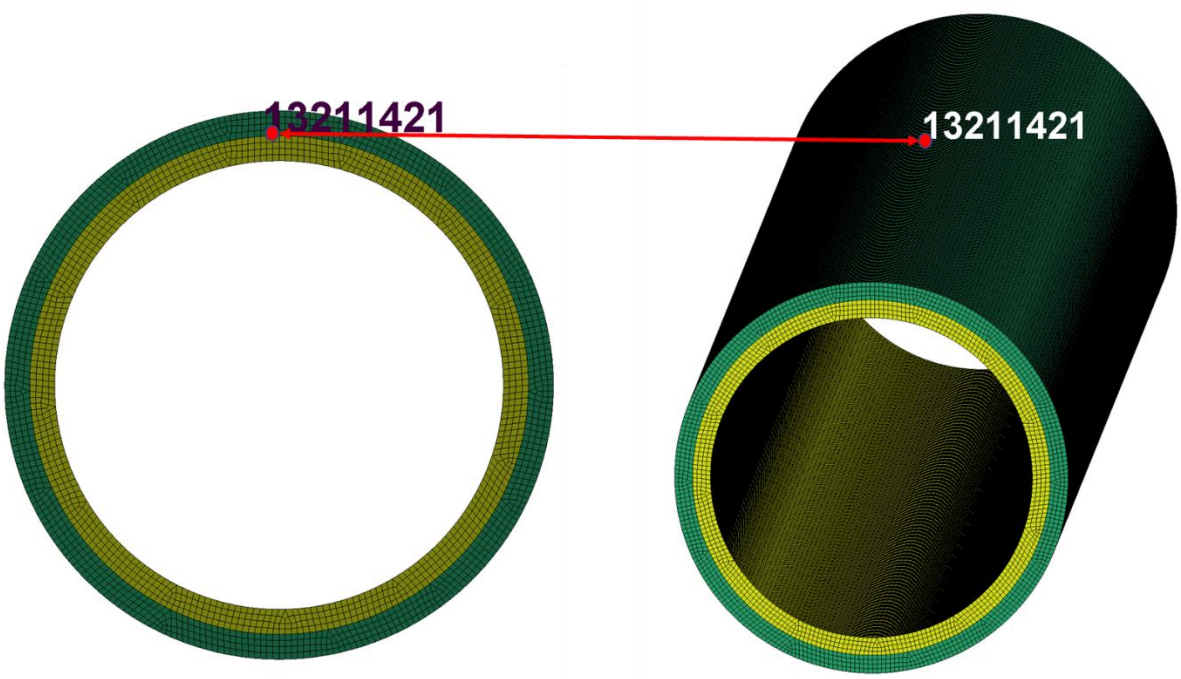

Figure 26 - Node position used to determine deformation of the pipeline

Other factors to consider were the pipeline protection and the seabed effect. Compared to an unprotected pipeline, a concrete coating was expected to help reduce the total deformation. A flexible seabed was also likely to reduce the amount of energy in the pipeline, reducing the deformation compared to a rigid seabed.

5.3.1 With Coating

Figure 27 below shows the deformation of the steel pipeline for cases 4-6. The flat impact resulted in the smallest deformation to the pipeline. This was due to a more significant impact area than the side and tip impact, resulting in a higher energy distribution and absorption from the container. The side impact had a slightly more significant deformation due to a smaller impact area. At 0.02 seconds, the tip impact had a positive displacement. This was because the chosen node was not directly where the tip of the container hit the pipeline first. When the tip hit the pipeline, the surrounding nodes would move upwards before starting to deform. Therefore, the tip impact had a positive displacement at 0.02 seconds before deforming to a little more than 0.6 mm. The tip impact had the most severe deformation. This is because it had the smallest impact area, which led to a more effortless penetration of the concrete coating and steel pipeline. These results support the assumption that the tip impact would give the largest deformation due to the small impact area.

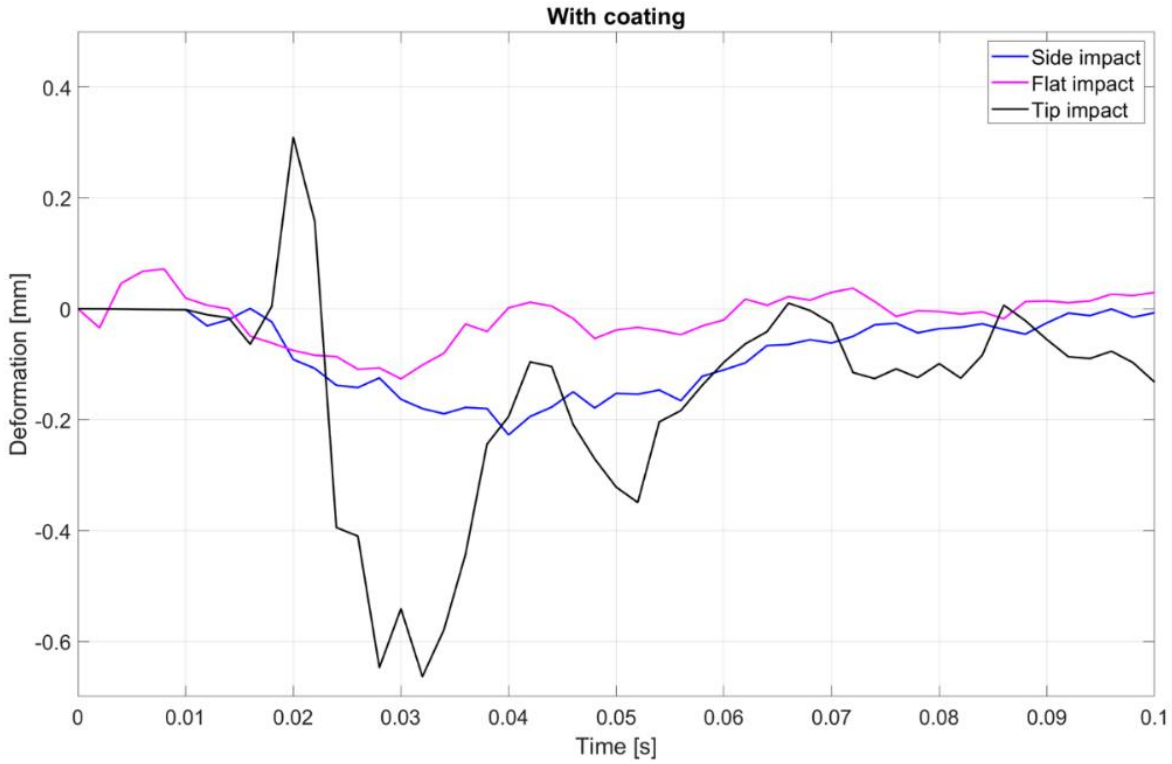

Figure 27 - Deformation of the pipeline with coating at node 13211421

Figure 28 below shows the different impact angles and how they affect the pipeline and container. The flat impact destroyed the pipeline in two places, along the edges of the container. This could be because the container frame is thicker and stiffer than the side walls, causing more damage to the pipeline in these two areas. For the side impact, both the container and the pipeline took some damage and were deformed. The tip impact destroyed the pipeline, resulting in the container going through the concrete and steel parts. For the tip impact scenario, the container did not deform much (see Figure 28). Hence, it does not absorb much of the energy. The same happened for the scenarios without coating protection, discussed in Chapter 5.3.2 below. Chapter 5.3.2 have further discussed why the container has so little deformation for the tip impact scenarios.

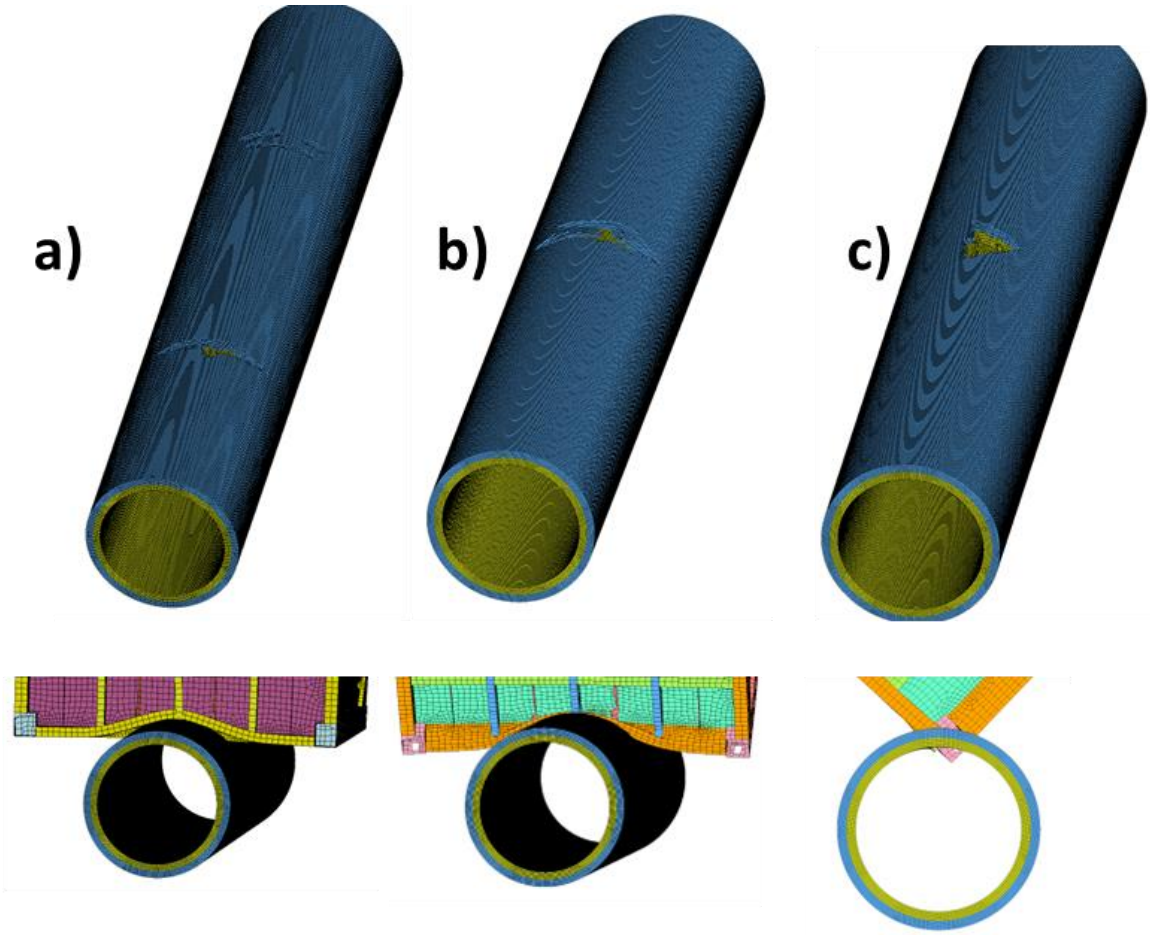

Figure 28 - Deformation of pipeline and container due to different impact positions: a) Flat Impact, b) Side Impact, c) Tip Impact [21]

5.3.2 Without Coating

Figure 29 below shows the deformation of impact scenarios 10-12. It can be observed that the smallest deformation was from the flat impact scenario. The most considerable deformation occurred in the tip impact scenario. Comparing the unprotected pipeline with the protected pipeline, the deformation was almost three times larger for the tip impact with an unprotected pipeline. The same occurs for the side impact, where the unprotected pipeline deformed nearly three times more than the protected pipeline. In the flat impact scenario, the unprotected pipeline deformed around four times more than the protected pipeline.

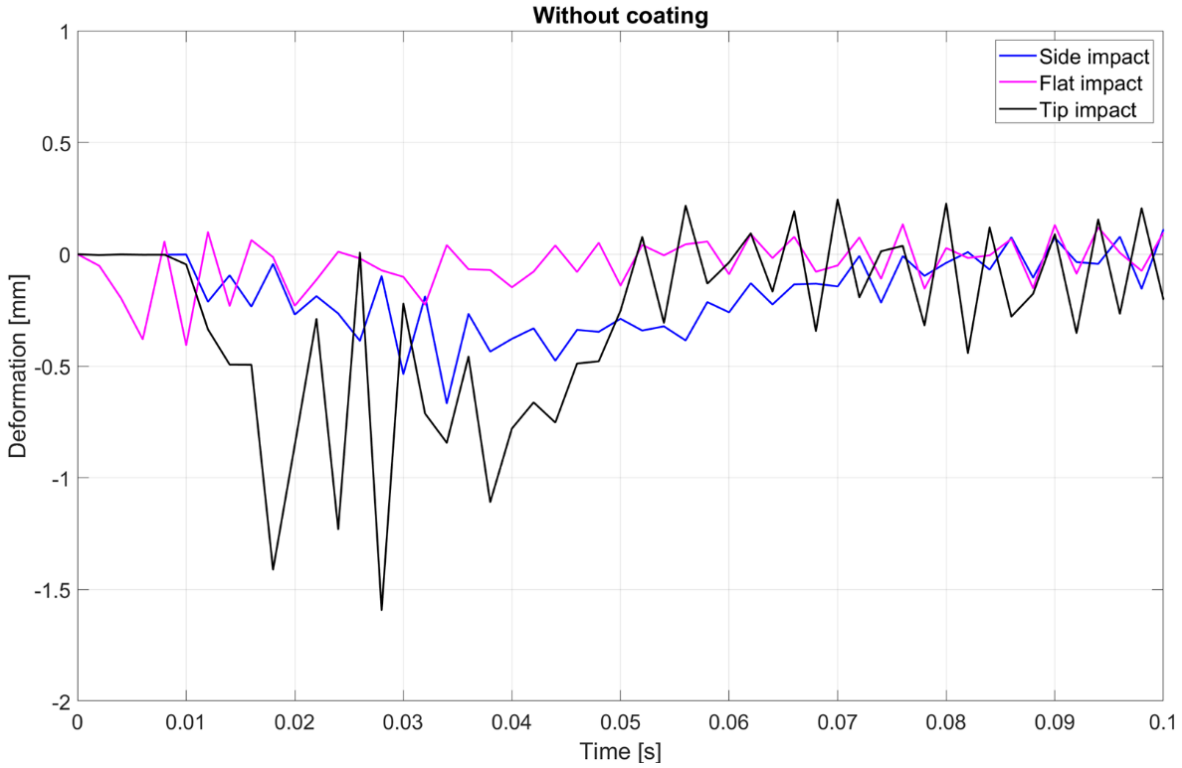

Figure 29 - Deformation of node 13211421 without coating

Figure 30 below shows the deformations of the pipeline and container at different impact positions. For the flat and side impact scenario there was slight deformation to the pipeline and more deformation to the container. The tip impact scenario penetrated the pipeline with little to no container deformation. This was unexpected, since the container was expected to have some deformation. One possible reason could be the big difference in mesh size between the pipeline and container. Another reason could be that most of the container has a yield strength of 355 MPa, while the pipeline has a weaker steel strength with a yield strength of 275 MPa.

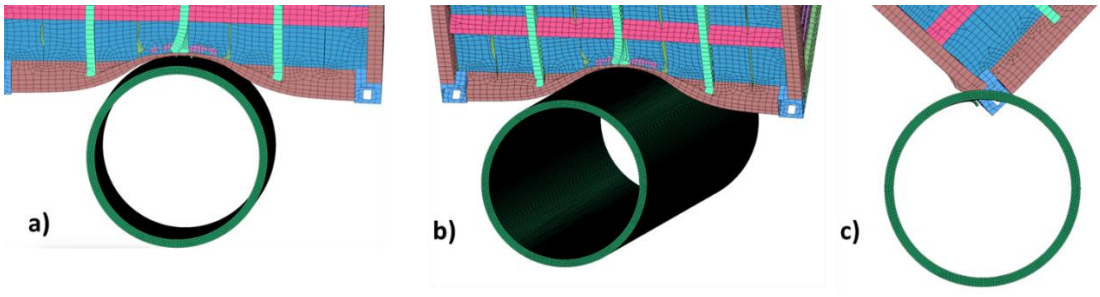

Figure 30 - Deformation of pipeline and container [21]

5.3.3 Flexible vs Rigid

The nodal displacement between a flexible and a rigid seabed was compared. A side impact onto an unprotected steel pipeline was used for both scenarios (cases 8 and 11). The results show the global nodal deformation for both scenarios. The rigid seabed had a maximum deformation of a little more than 0.5 mm, while the flexible seabed model had a deformation closer to 2 mm. These results were unexpected, since it was assumed the scenario with a rigid seabed would give more severe deformations. However, since this was a global analysis, it shows the total deformation of the nodal point. In case 11, the rigid seabed stopped the pipeline from moving downwards and the pipeline could only deform locally. Case 8, with the flexible seabed, allowed the pipeline to move downwards in the seabed, in addition to a small local nodal deformation. This explains why the model with a flexible seabed received the highest deformation, since it combined both local and global deformation.

However, the scope of this test was to compare the local deformations and not the global. If the test had been performed as intended by only looking at the local deformation of the nodes, the results would probably have been more in accordance with expectations.

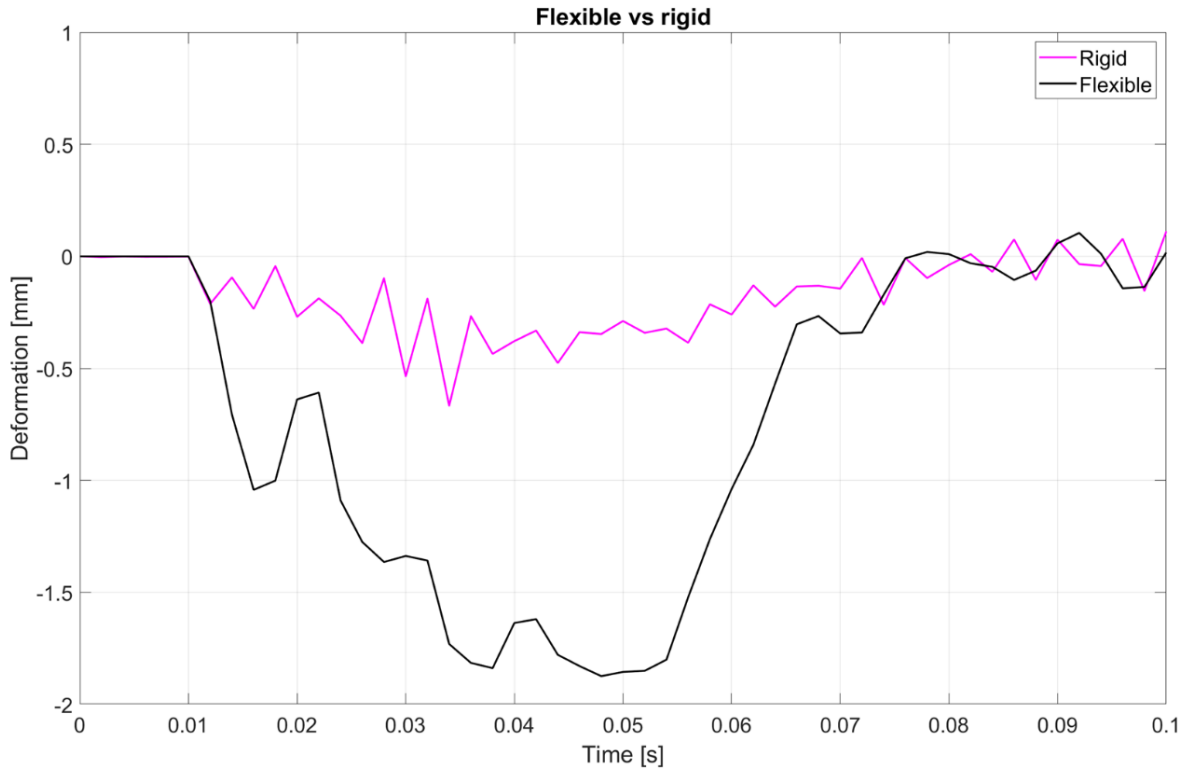

Figure 31 – Deformation of node 13211421, flexible vs rigid seabed

5.4 Internal Energy

Impact scenarios 3, 4-6, 9 and 10-12 have been used in this comparison. Internal energy can be defined as the total energy of a closed system [31]. The total energy is the sum of an object's potential and kinetic energy. In this chapter, the internal energy of the pipeline due to a container impact has been further studied. The internal energies can be found by defining a contact between the container and the pipeline. The container will carry the same potential energy in all scenarios since it has the same mass and velocity. However, the size of the impact area will vary for the different impact angles. Since the tip impact has the smallest area of impact, it is expected to result in the highest internal energy on the pipeline. A. Ramberg's study on a dropped object onto an offshore installation has also examined the effect of different impact positions [6]. The study concludes that the damage to the pipeline was highly dependent on the size of the impact area of the dropped object.

5.4.1 With Coating

Impact scenarios 4-6 were used in this comparison. Figure 32 shows a big difference in internal energy between the different impact positions. The flat- and side impact resulted in almost no internal energy for the pipeline compared to the tip impact. This may be due to the impact area of the different positions. The tip impact had some pointy punching impact that would hit at one specific point, whereas the other two had a more significant impact area. That may be the reason for the difference in the results. Since the internal energy for the flat and side impact are low, it suggests that the container absorbs most of the energy. The tip impact scenario indicates that the pipeline absorbs more energy, leading to a smaller container deformation.

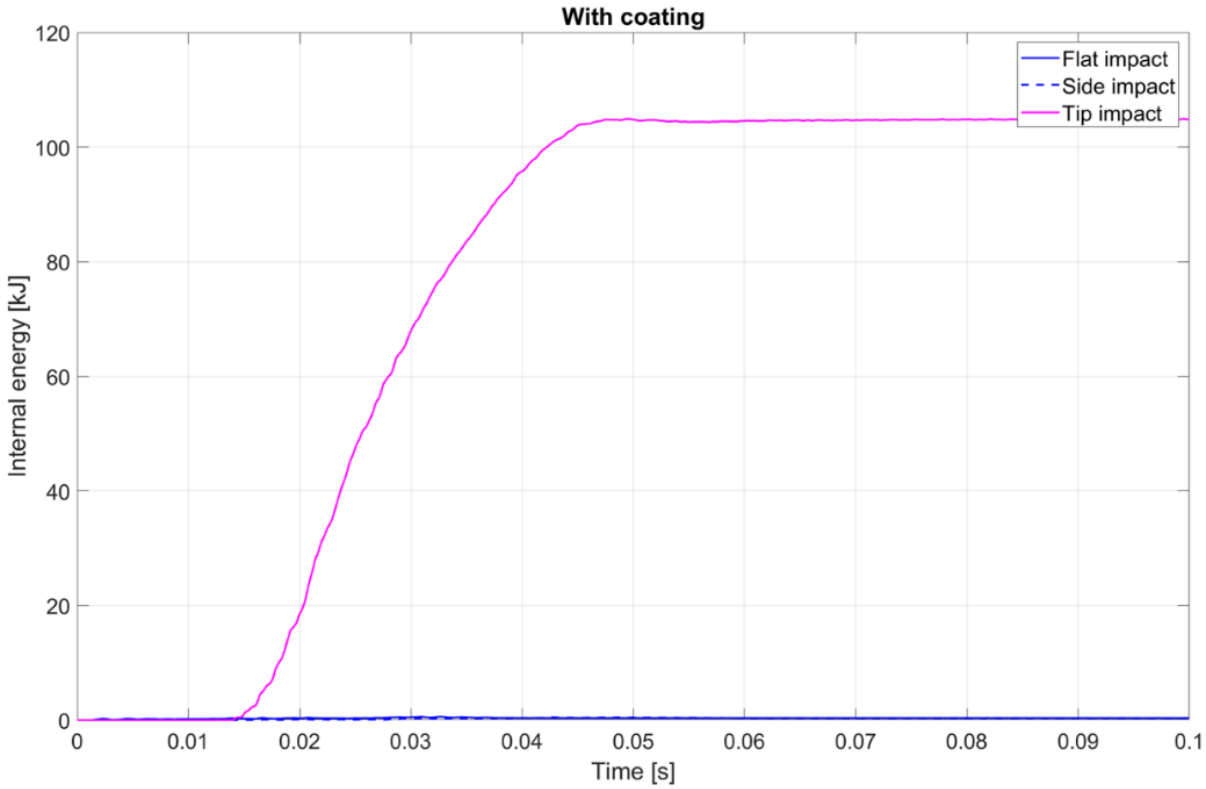

Figure 32 - Internal energy of steel pipeline with coating

5.4.2 Without Coating

Impact scenarios 10-12 have been used in this comparison. The flat and side impact scenarios resulted in a low internal energy in the steel pipeline. The tip impact had a greater internal energy. Like the scenario with a protective layer of concrete coating, the tip impact resulted in significantly higher internal energy of the steel pipeline. As mentioned in the other scenario, most of the internal energy for the flat and side impact was absorbed by the container, while the pipeline absorbed more internal energy for the tip impact. When comparing the tip impact scenario for a pipeline with and without coating, the internal energy was higher for an unprotected pipeline.

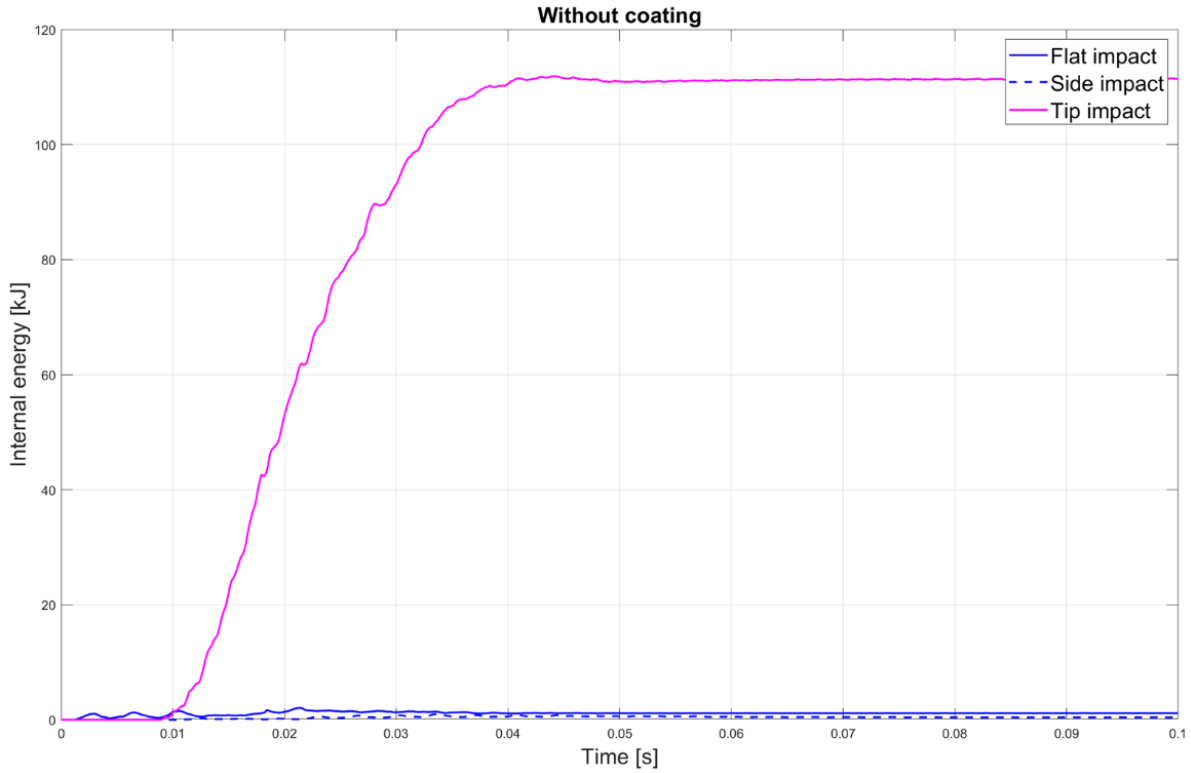

Figure 33 - Internal energy of steel pipeline without coating

5.4.3 Flexible vs Rigid Seabed

A comparison between a flexible and rigid seabed has also been made. The flexible and rigid seabed have both been compared for the scenarios with and without coating protection. Figure 34 shows the internal energy of the steel pipeline for scenarios 3, 6, 9 and 12.

The impact scenarios with a coating protection had a lower internal energy both for the flexible and rigid seabed, compared to the two scenarios without a coating protection. When comparing the effect of the seabed for the scenarios with a coating protection, the effect of the flexible seabed resulted in a lower internal energy of the pipeline than the rigid. This is because the flexible seabed absorbs some of the energy, which the rigid seabed does not.

The impact scenarios without coating protection generally had a higher internal energy of the pipeline. Surprisingly, when comparing the scenarios without coating protection, the effect of a flexible seabed acted opposite compared to the impact scenario with coating protection. The impact scenario with a flexible seabed resulted in a slightly higher internal energy of the pipeline, compared to the rigid seabed scenario. A reason for this surprising result, could be

down to an error in the model, since it was expected that the effect of a flexible seabed would help reduce the internal energy on the pipeline.

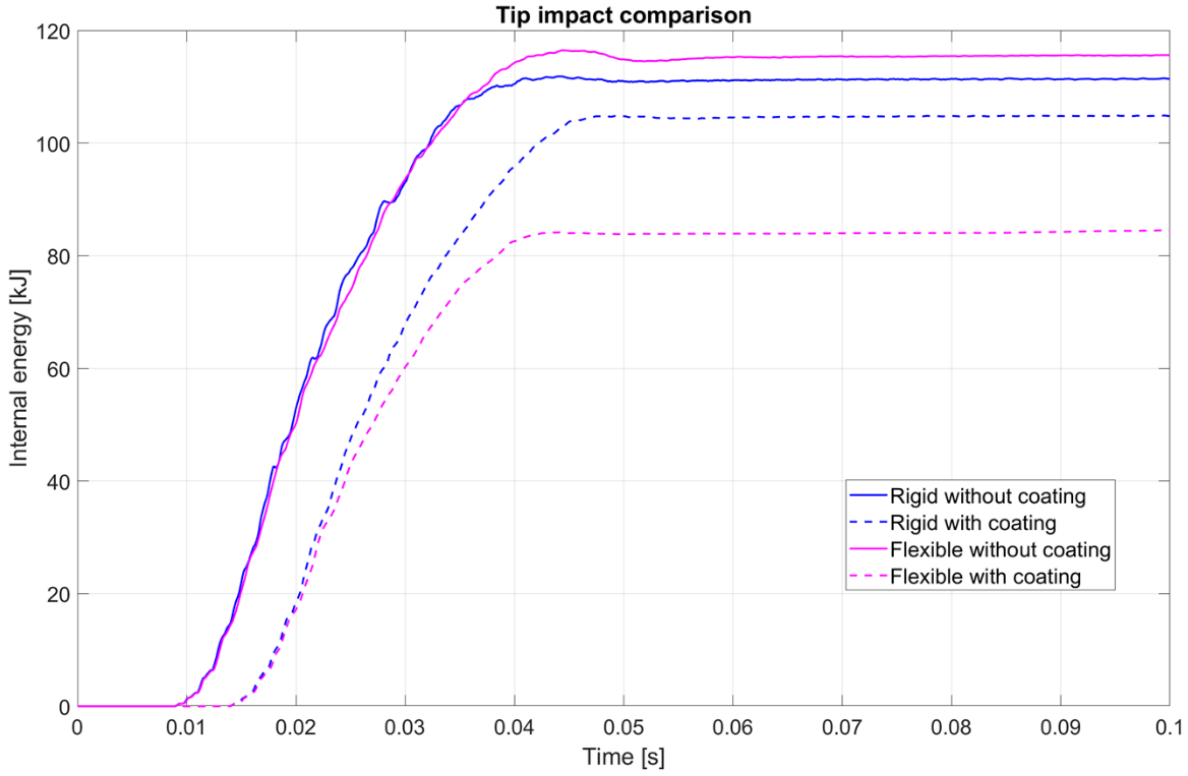

Figure 34 - Internal energy of steel pipeline, flexible vs rigid seabed

5.5 Steel Grade of the Pipeline

The pipeline has been compared with two different steel grades, S275 and S355, for the same container impact scenario. The impact scenarios used were cases 6 and 13. The increase in the pipeline's steel grade was expected to result in a lower internal energy and less deformation of the pipeline. This is because a stiffer pipeline is expected to absorb less energy, resulting in more energy being absorbed by the container. The impact force has also been compared. The steel grade properties may be seen in Tables 10 and 11. The red square shows the yield strength of the steel, and the green square indicates the stress-strain values for each material. The stress-strain values have been used to plot the two stress-strain curves (see Figure 9 in Chapter 4.5.1).

Table 10 - S355 steel grade of the steel pipeline [21]

TITLE							
Steel							
1 MID	RO	E	PR	SIGY	ETAN	FAIL	TDEL
1	7800.0000	2.000e+011	0.3000000	3.550e+008	7.300e+008	0.2500000	0.0
2 C	P	LCSS	LCSR	VP	LCF		
0.0	0.0	0	0	0.0	0		
3 EPS1	EPS2	EPS3	EPS4	EPS5	EPS6	EPS7	EPS8
0.0	0.0097000	0.0645000	0.1290000	0.2580000	0.3870000	0.4644000	0.4773000
4 ES1	ES2	ES3	ES4	ES5	ES6	ES7	ES8
3.550e+008	3.550e+008	4.386e+008	4.840e+008	5.225e+008	5.225e+008	4.840e+008	9.675e+007

Table 11 - S275 steel grade of the pipeline [21]

TITLE							
Steel							
1 MID	RO	E	PR	SIGY	ETAN	FAIL	TDEL
1	7800.0000	2.000e+011	0.3000000	2.750e+008	7.300e+008	0.2500000	0.0
2 C	P	LCSS	LCSR	VP	LCF		
0.0	0.0	0	0	0.0	0		
3 EPS1	EPS2	EPS3	EPS4	EPS5	EPS6	EPS7	EPS8
0.0	0.0075000	0.0500000	0.1000000	0.2000000	0.3000000	0.3600000	0.3700000
4 ES1	ES2	ES3	ES4	ES5	ES6	ES7	ES8
2.750e+008	2.750e+008	3.400e+008	3.750e+008	3.950e+008	4.050e+008	3.750e+008	7.500e+007

5.5.1 Internal Energy

The internal energy curve in Figure 35 shows the difference in internal energy between the two materials. As expected, using the S275 results in higher internal energy in the steel than using the S355 steel grade. Due to S355 being a more robust steel grade, it absorbed less of the total energy resulting in more deformation to the container. Since the S275 steel had a lower yield strength, it absorbed more of the internal energy, which should result in a greater deformation than the S355 steel.

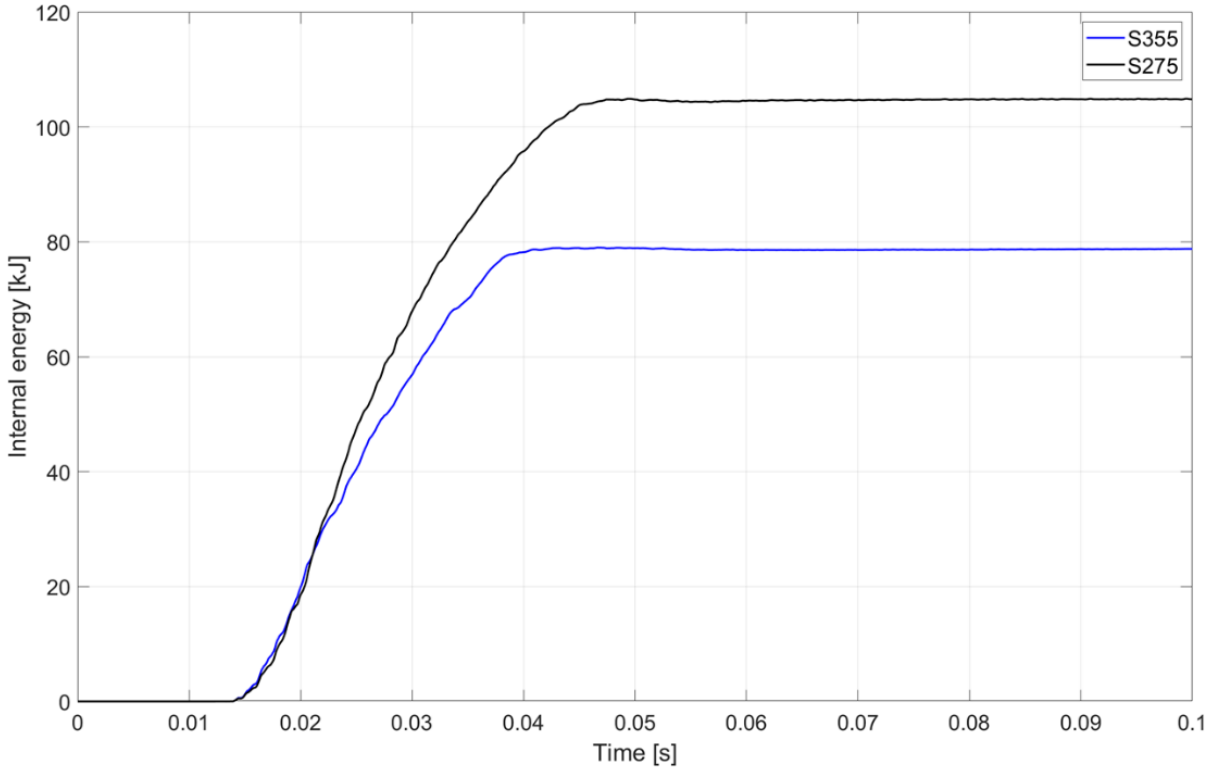

Figure 35 - Internal energy of pipeline for different material grades

5.5.2 Impact Force

Figure 36 below shows the impact force and how it performs for the pipeline's two different material steel grades. There were no significant differences between the curves. The blue curve had a slightly higher peak value than the black curve, while the black curve had a bigger variation between a drop and a peak value. As mentioned in Chapter 5.2.1, a large difference between a peak value and the subsequent drop suggests that a part of the element is being destroyed. Therefore, it made sense that there was more damage to the S275 steel than to the S355 steel with the same impact force.

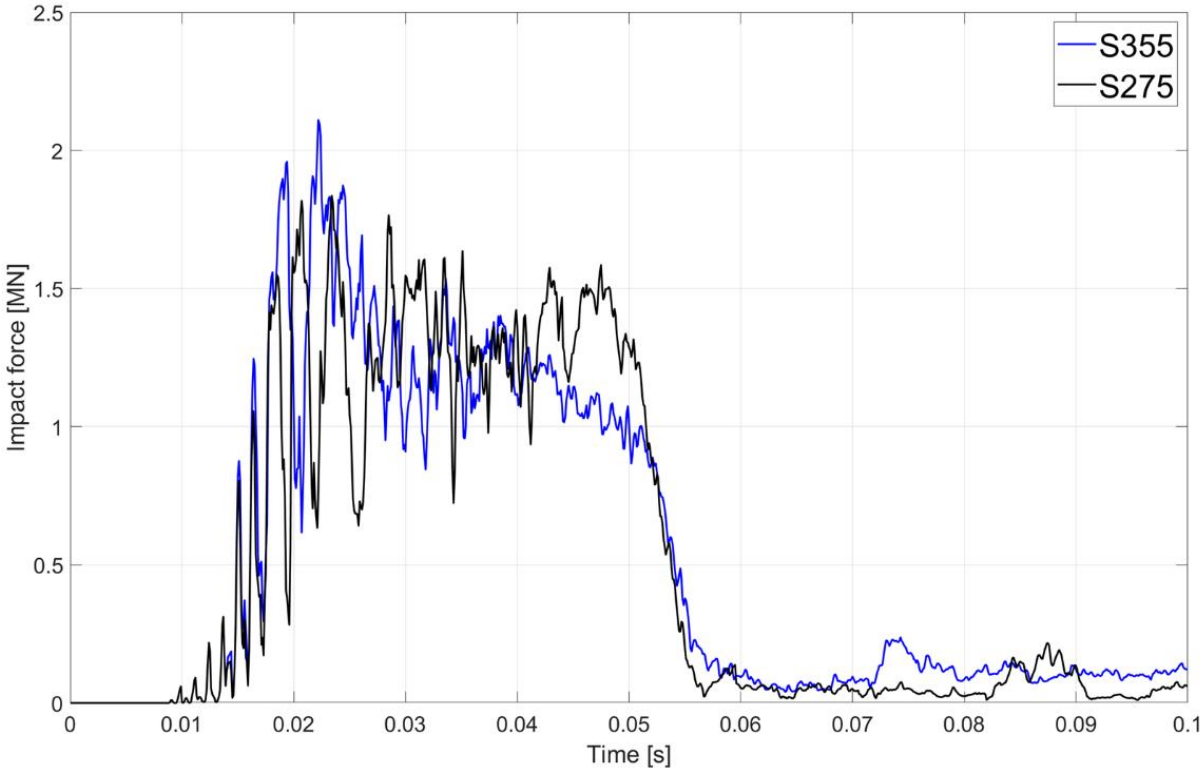

Figure 36 - Impact force of pipeline for different material grades

5.5.3 Deformation

The deformation has also been checked for both steel material types. Figure 37 below shows that the pipeline with S275 steel grade deforms more than the pipeline with S355 steel grade. The result from the deformation supported earlier claims that the S275 should have a larger deformation than the S355 due to the lower yield strength of the material. Therefore, if it was desired to reduce the deformation of a pipeline, one solution could be to increase the yield strength of the material.

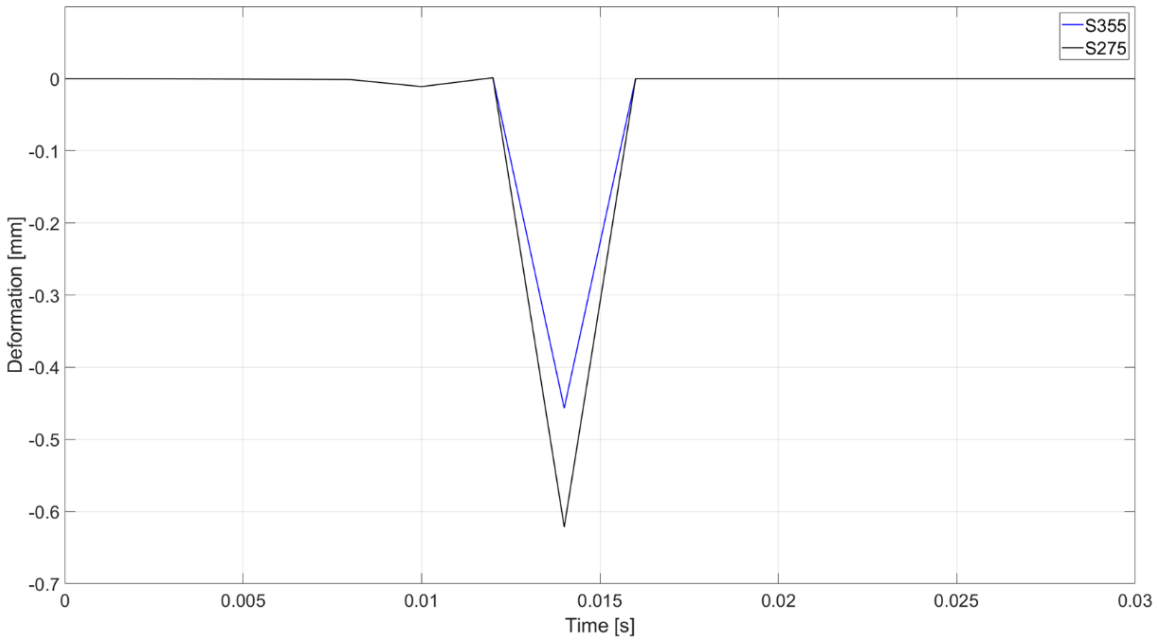

Figure 37 - Deformation of the pipeline for different material grades

6 Conclusion

The thesis has assessed the structural response from a dropped object impact onto a subsea pipeline. LS-DYNA has been utilised to run non-linear finite element analyses of the impact. A dynamic simulation was used to perform all the studies where the container and pipeline were deformable. Convergence tests have been performed with the container being rigid. The impact scenarios were analysed by comparing different factors such as internal energy, impact force, and deformation. Various parameters were considered, including the angle of impact, the flexibility of the seabed, steel grade, and the presence or absence of concrete coating. These parameters were varied and compared in the different impact scenarios.

The convergence tests provided information on the mesh size required in the analyses. Both internal energy, impact force and the deformation showed how the results would vary with different mesh sizes. For both internal energy and impact force, the results showed that the 6.25 mm and 12.5 mm mesh were closer to each other than the 25 mm mesh. The deformation was almost identical for the 6.25 and the 12.5 mm, while the 25 mm had a much larger deformation. Based on these results, the conclusion was to use the 12.5 mm mesh size because it is accurate enough, and a smaller mesh size would create problems regarding computational time.

The results of the analysis show how the impact force varies with the three different impact angles of the container. Based on the impact force and how the force curves look, the tip impact would be the scenario that created the most extensive damage to the pipeline. This was because it had the highest impact force for the scenario with coating and was slightly lower than the flat impact for the scenario without coating. This would be the worst since the impact area was much smaller on the tip impact. When comparing the scenario with a coating to the one without, the scenario with coating had a slightly higher impact force. The results were similar between the flexible seabed and the rigid.

The deformation was larger for the scenarios without coating compared to the scenarios with coating protection of the pipeline. This was because the coating would protect the pipeline and reduce the internal energy, resulting in a lower total deformation than the unprotected pipeline. The flexible seabed had a larger global deformation. The seabed was soft, which resulted in a larger global pipe deformation. The scope of the test was to compare the local deformation and not the global. Had the test been conducted as originally intended, focusing on the local

deformation of the nodes, it is likely that the results would have aligned more closely with the expected outcomes.

In comparison to the tip impact, the flat and side impact scenarios inflicted minimal internal energy to the pipeline. The higher deformation observed in the container during the flat and side impact scenarios indicates that a significant portion of the internal energy was absorbed by the container itself. On the other hand, the container underwent minimal deformation in the tip impact scenario, leading to a greater transfer of internal energy to the pipeline. The presence of a flexible seabed resulted in some energy absorption to the pipeline, particularly noticeable in the scenario where the container had a coating. Surprisingly, in the scenarios without coating protection, the effect of a flexible seabed demonstrated opposite behaviour compared to the impact scenarios with coating protection. The scenario involving a flexible seabed exhibited a slightly higher internal energy in the pipeline when compared to the scenario with a rigid seabed.

Two different steel grades in the pipeline have been compared to investigate their impact on the results. The internal energy was lower for the higher-strength steel (S355) than the lower-strength steel (S275). This was expected because higher-strength steel would be more robust, resulting in higher energy absorption to the container. The deformation also acted as expected, with the S275 having a more considerable deformation due to its lower strength. As explained earlier, the impact force showed that the S275 steel received more extensive damage than the S355.

7 Further studies

For further studies, there is a lot more to consider regarding dropped objects. Due to limited time it had to be prioritised what cases and parameters to investigate. Some examples of things not investigated will be further addressed here.

Firstly, one could utilise restart analysis or dynamic relaxation techniques to incorporate gravity loads into the models. This would allow for a more comprehensive system analysis under realistic conditions.

Another possibility would be to explore running simulations with varying thicknesses of the pipeline and the protective measures in place. By examining the effects of different thicknesses, researchers can gain insights into the structural integrity and vulnerability of the pipeline under different scenarios.

For this thesis, only one protection method has been assessed. Other protection methods, such as polymer coating or concrete blankets, could be interesting to analyse and, compared to, for example, concrete coating.

The analysis did not include an assessment of other dropped objects, such as a tank or a pipeline. Including these objects in the study could provide valuable insights into the dynamic response of the pipeline.

In addition, experimenting with different material properties can provide valuable information. By varying the properties of the materials involved, such as the pipeline and the container, researchers can assess the impact of these variations on the overall behaviour of the pipeline and the dropped object.

Furthermore, running simulations at various velocities and subsequently comparing the results would be interesting. This would be beneficial to see how the dynamic response changes with different velocities.

A model could be created to better understand the system's behaviour where the container is considered rigid and compared with a deformable container.

Investigating different steel grades for the pipeline and the container would be valuable. Assessments on the structural performance and failure mechanisms can be performed by varying the material steel grade of the container.

Lastly, it would be worthwhile to examine the energy absorption capabilities of the container. Understanding how the container dissipates and absorbs energy during impact scenarios is crucial for designing effective protective measures and ensuring the system’s safety.

References

[1] Gong Xiang, Kunpeng Rao, Xianbo Xiang, and X. Yu, "Overview and analysis on recent research and challenges of dropped objects
in offshore engineering," *Ocean Engineering,* 2023.

[2] Y. Tian *et al.*, "Assessment of submarine pipeline damages subjected to falling object impact considering the effect of seabed," *Marine Structures,* vol. 78, p. 102963, 2021.

[3] DNVGL-RP-F107, "Risk assessment of pipeline protection," 2017.

[4] DNVGL-RP-C204, "Design against accidental loads," 2017.

[5] Z. Liu and A. K. Verma, "A novel toolbox for dropped object hit probability evaluation and orientation optimization of subsea lines," *International Journal of System Assurance Engineering and Management,* vol. 13, no. 4, pp. 1705-1713, 2022.

[6] A. Ramberg, "Analysis of Dropped Objects on Offshore Installations," NTNU, 2022.

[7] F. Jiang, S. Dong, Y. Zhao, Z. Xie, and C. G. Soares, "Investigation on the deformation response of submarine pipelines subjected to impact loads by dropped objects," *Ocean Engineering,* vol. 194, p. 106638, 2019.

[8] M. R. U. Kawsar, S. A. Youssef, M. Faisal, A. Kumar, J. K. Seo, and J. K. Paik, "Assessment of dropped object risk on corroded subsea pipeline," *Ocean Engineering,* vol. 106, pp. 329-340, 2015.

[9] Z. Liu and A. K. Verma, "A novel toolbox for dropped object hit probability evaluation and orientation optimization of subsea lines," 2021.

[10] A. Bergstad, "Assesment of HUll Repsonse due to Impact from Falling Object," NTNU-Trondheim, 2014.

[11] Y. Sha, "Lecture 9 - ship collision with tubular members," Canvas - Universitet i Stavanger.

[12] Robert D. Cook, David S. Malkus, Michael E. Plesha, and R. J. Witt, *Concepts and Applications of Finite Element Analysis*. John Wiley & Sons Inc, 2001, p. 736.

[13] A. Harish. "What is Convergence in Finite Element Analysis?" https://www.simscale.com/blog/convergence-finite-element-analysis/ (accessed.

[14] Ansys. "Ansys LS-DYNA." https://www.ansys.com/products/structures/ansys-ls-dyna (accessed 2023).

[15] Oasys-software. "LS-DYNA." https://www.oasys-software.com/dyna/software/ls-dyna/ (accessed 26.01.23, 2023).

[16] Dynamore. https://www.dynamore.de/en/products/pre-and-postprocessors/prepost (accessed 2023).

[17] NetApp. "What is high performance computing?" https://www.netapp.com/data-storage/high-performance-computing/what-is-hpc/ (accessed 14.03.23.

[18] A. R. C. (ARC). "What is high performance computing?" https://www.usgs.gov/advanced-research-computing/what-high-performance-computing (accessed.

[19] N. r. i. services. "Fram." https://documentation.sigma2.no/hpc_machines/fram.html (accessed 2023).

[20] Y. Sha, Z. Liu, J. Amdahl, and C. Dørum, "Simulation of shipping container impact with bridge girders," in *The 30th International Ocean and Polar Engineering Conference*, 2020: OnePetro.

[21] K. U. S. MANUAL, "LS-DYNA," 1992.

[22] M. Abedini and C. Zhang, "Performance assessment of concrete and steel material models in ls-dyna for enhanced numerical simulation, a state of the art review," *Archives of Computational Methods in Engineering,* vol. 28, pp. 2921-2942, 2021.

[23] M. Esmaeili and B. Tavakoli, "Finite element method simulation of explosive compaction in saturated loose sandy soils," *Soil Dynamics and Earthquake Engineering,* vol. 116, pp. 446-459, 2019.

[24] Y. D. Murray, A. Y. Abu-Odeh, and R. P. Bligh, "Evaluation of LS-DYNA concrete material model 159," United States. Federal Highway Administration. Office of Research …, 2007.

[25] L.-D. support. "Contact modelling in LS-DYNA." https://www.dynasupport.com/tutorial/ls-dyna-users-guide/contact-modeling-in-ls-dyna (accessed.
[26] Simscale. "What Are Boundary Conditions?" https://www.simscale.com/docs/simwiki/numerics-background/what-are-boundary-conditions/ (accessed.
[27] J. D. Reid, "LS-DYNA examples manual," p. 159, 1998. [Online]. Available: https://www.dynasupport.com/manuals/additional/ls-dyna-examples-manual.
[28] Y. Kulkarni, "Development of algorithms for generating connected midsurfaces using feature information in thin-walled parts," ed, 2017.
[29] E. Kuusisto. "SHELLS vs. SOLIDS | Finite Element Analysis Quick Review." https://www.linkedin.com/pulse/shells-vs-solids-finite-element-analysis-quick-review-kuusisto-p-e-/ (accessed.
[30] M. M. T. Duncan. "The Fundamentals of FEA Meshing for Structural Analysis." Ansys. https://www.ansys.com/blog/fundamentals-of-fea-meshing-for-structural-analysis (accessed 2023).
[31] T. E. o. E. Britannica, "potential energy," 2023. [Online]. Available: https://www.britannica.com/science/potential-energy.